

7-2015

FRET Study of Ligand Binding and Exchange Kinetics on the Surface of CdSe/ZnS Quantum Dots

Randee Jean McBride
University of Arkansas, Fayetteville

Follow this and additional works at: <http://scholarworks.uark.edu/etd>

 Part of the [Physical Chemistry Commons](#)

Recommended Citation

McBride, Randee Jean, "FRET Study of Ligand Binding and Exchange Kinetics on the Surface of CdSe/ZnS Quantum Dots" (2015). *Theses and Dissertations*. 1267.
<http://scholarworks.uark.edu/etd/1267>

This Thesis is brought to you for free and open access by ScholarWorks@UARK. It has been accepted for inclusion in Theses and Dissertations by an authorized administrator of ScholarWorks@UARK. For more information, please contact scholar@uark.edu, ccmiddle@uark.edu.

FRET Study of Ligand Binding and Exchange Kinetics on the Surface of CdSe/ZnS Quantum
Dots

A thesis submitted in partial fulfillment
of the requirements for the degree of
Masters of Science in Chemistry

by

Randee McBride
Northeastern State University
Bachelor of Science in Chemistry, 2011

July 2015
University of Arkansas

This thesis is approved for recommendation to the Graduate Council

Dr. Colin Heyes
Thesis Director

Dr. Bill Durham
Committee Member

Dr. Jingyi Chen
Committee Member

ABSTRACT

Quantum dots are a valuable tool in many research applications and commercial development. Their applications are far reaching and as such have become a topic of great interest. One of their greatest assets is the ability to utilize them as water soluble fluorescent labels. Rendering the nanocrystals water soluble can be accomplished in several ways, but one very popular method is by capping them with water-soluble multi-functional organic ligands. However, these ligands, when attached to the quantum dot surface, are labile and can be exchanged which can be problematic when using the quantum dots in research applications. This project investigates the mechanisms of the exchange of surface bound ligands by employing modified fluorescent dyes as probes. The kinetics of the exchange is quantified by studying the quenching of the quantum dot signal as a function of time caused by bound dyes through Förster resonance energy transfer. Quantum dots with various ligands of different size, charge, and coordination are exposed to water-soluble dyes of different charges. Overall, it was discovered that a multi-component mechanism of exchange is present. The rate of the first very fast components provide insight into the initial binding of ligands to the surface, while the longer component(s) provides information about the exchange of ligands by dyes on the surface of the quantum dot.

ACKNOWLEDGEMENTS

I would like to thank my Master's thesis advisor Dr. Colin Heyes for allowing me to join his research group and for providing me with guidance and encouragement throughout my years at the University of Arkansas. I would also like to express my appreciation for the support I have been given by all of the members of the Heyes Research Group. Thank you to past members Hiroko Takeuchi and Dr. Benard Omogo for teaching me the ropes and to postdoctoral researcher Dr. Feng Gao for always being willing to help. I am also very appreciative of Dr. Bill Durham and Dr. Jingyi Chen for serving on my advising committee. I'd like to thank my mother and father, Lori and Jess McBride, for their unconditional support in all of my endeavors. I am also grateful for my sister Jessie McBride, who I know is always just a phone call away. Finally, thank you Valerie McKinney for talking me into going to grad school in the first place. It was worth it.

DEDICATION

This finished work and the time it represents is dedicated to Eric Casady, who sacrificed years so that I may pursue the wonderful opportunity that was offered to me. Thank you for supporting me, encouraging me, and for your unerring belief in me. It means more to me than I can express.

TABLE OF CONTENTS

I. Chapter 1: Introduction and Background	
1.1 Quantum Dots: Definition and Mechanism	1
1.2 Quantum Dots: Characterization	2
1.2.1 FRET	3
1.3 Quantum Dots: Development	5
1.4 Purpose	8
1.5 CdSe/ZnS Quantum Dots	9
1.6 Ligands	10
1.7 Fluorescent Dyes	11
1.7.1 SATA	12
II. Chapter 2: Experimental Methods	
2.1 Quantum Dot Characterization	13
2.2 Quantum Dot Purification	13
2.3 Ligand Exchange and Phase Transfer	14
2.3.1 Mercaptopropionic Acid (MPA)	14
2.3.2 D-penicillamine (DPA)	15
2.3.3 Dihydrolipoic Acid (DHLA)	15
2.4 QD-Ligand in Water Concentration	16
2.5 Dye Modification with SATA	17
2.6 Dye Characterization	18
2.7 Fluorescence	18
III. Chapter 3: Results and Discussion	
3.1 Characterization of PROMO 700	20
3.2 Atto 700	20
3.3 PromoFluor 700	24
3.4 Future Outlook	46
3.5 References	47

LIST OF ABBREVIATIONS

ATTO	Atto 700 Amine
CdSe	Cadmium Selenide
DHLA	Dihydrolipoic Acid
DPA	D-penicillamine
FRET	Förster Resonance Energy Transfer
FWHM	Full Width at Half Max
HLPC	High Performance Liquid Chromatography
MALDI-TOF	Matrix Assisted Laser Desorption-Ionization Time-Of-Flight
MPA	Mercaptopropionic Acid
ODA	Octadecylamine
PL	Photoluminescence
PBS	Phosphate Buffered Saline
PL	Photoluminescence
PROMO	PromoFluor 700 Amino-Modified
QD	Quantum Dot
SATA	N-Succinimidyl S-Acetylthioacetate
TMAOH	Tetramethylammonium Hydroxide Pentahydrate

UV-Vis

Ultraviolet-Visible Spectroscopy

ZnS

Zinc Sulfide

Chapter 1: Introduction and Background

1.1 Quantum Dots: Definition and Mechanism

Quantum dots are spherical nanocrystals that range in size from 2-10 nanometers in diameter [1]. One common class of quantum dots are fluorescent nanocrystalline semiconductors that have a composition primarily made up of atoms from groups II-VI or III-V [2]. The electronic and optical properties of these materials are dependent on their size as a result of quantum confinement [3]. The small spherical shape of QDs can approach that of the Bohr's radius, or the radius of the lowest energy electron orbit of a Hydrogen atom, resulting in an excited (delocalized) electron being confined in all three dimensions [4]. When the radius of the particle becomes smaller than the exciton Bohr radius, there is quantization of energy levels and the energy difference between the valence and conduction band (band gap) increases [5].

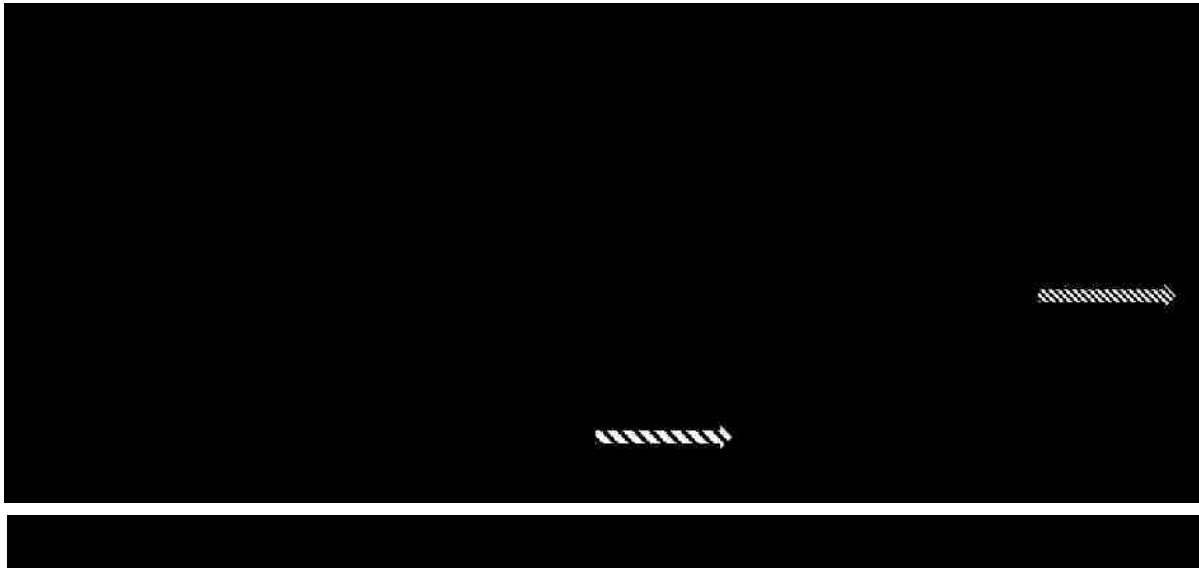
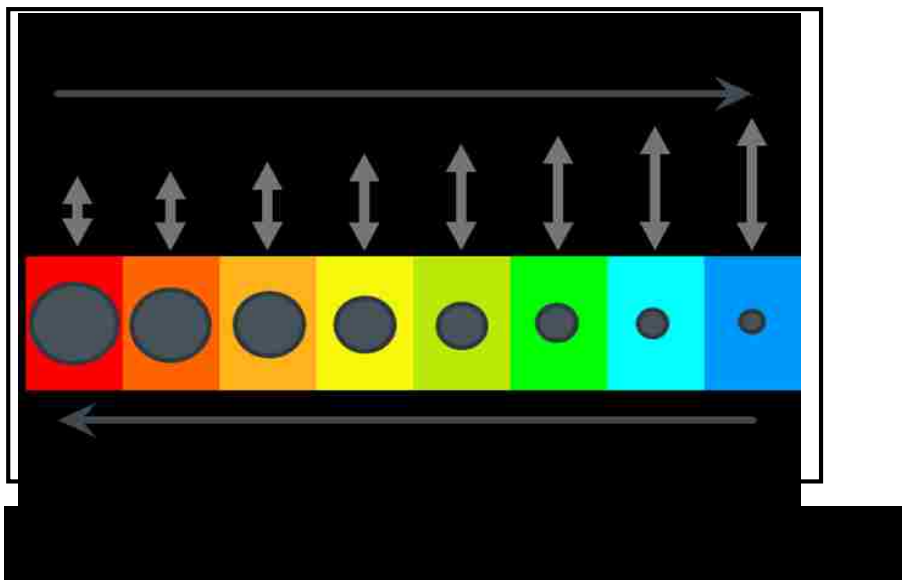


Figure 1 illustrates the process for photon absorption and emission in QDs. The emission of light comes from an electron hole pair. When the QD is excited, a photon promotes an electron to the conduction band, which leaves a “hole” in the valence band. Both the electron and the hole then

relax non-radiatively to the lowest allowed energy level in each band. From there the electron will recombine with the hole. This relaxation emits a lower-energy photon. A smaller sized particle has a larger band gap, which means that more energy is needed for excitation and more energy is released from relaxation to the ground state. This is the underlying reason that QDs can be made to emit light at different color wavelengths from red to blue with decreasing size (Figure 2). The color that the QDs emits is thus easily tunable by the size of the QD. This is done experimentally



by controlling the temperature and time of the synthesis process [6]. Often, the optical and structural stability of QDs are increased by adding a shell material that passivates surface trap states on the quantum dot [7].

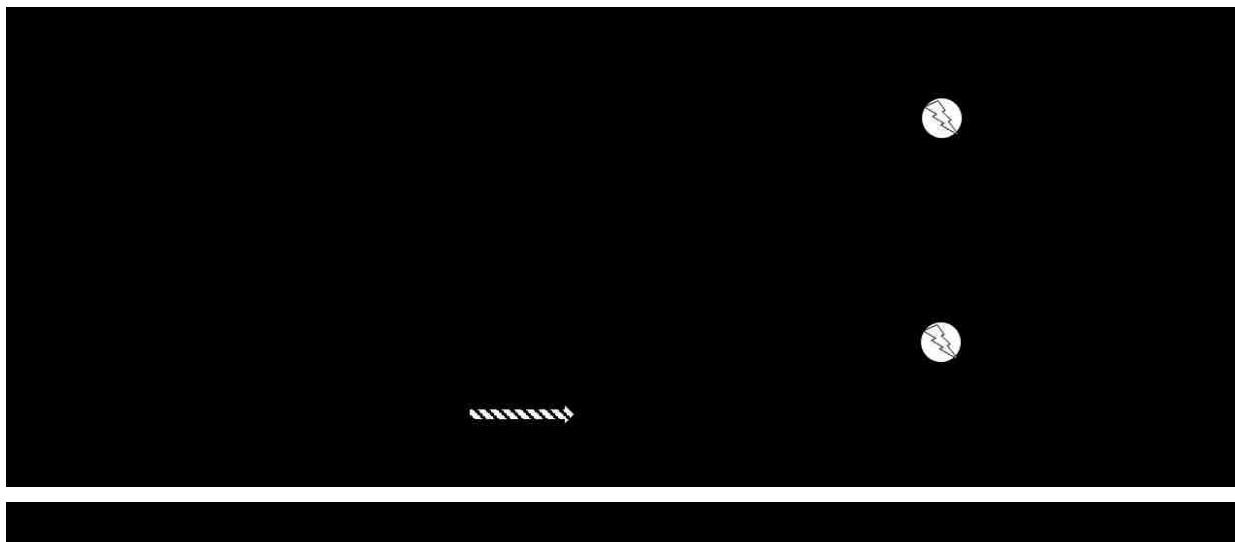
1.2 Quantum Dots: Characterization

QDs are being used for many applications which require different methods and instrumentation for data collection. When considering work done in characterization, bioanalysis, and bioimaging, the techniques for working with QDs are numerous. For example, in one study that investigated QD encapsulation and coating strategies with various ligands and polymers, the structural and colloidal characterization was made using dynamic light scattering, zeta potential,

and transmission electron microscopy [8]. The data gathered from these measurements provided information on the nanoparticle hydrodynamic size, the surface charges created by the polymers and ligands, and qualitative information for evaluating the structure of the QDs. Biological applications, such as tumor cell targeted imaging, can utilize QDs as fluorescent probes by measuring labeled cells with laser confocal scanning microscopy [9]. There are a few other techniques that are important to note, as they will be utilized in the research done here. The simplest tools for characterizing QDs are the absorption and emission spectra collected by Ultraviolet-Visible Spectroscopy (UV-Vis) and Photoluminescence Spectroscopy (PL). This data can provide information on bandgap energy, size of nanoparticles, and trap states caused by imperfections or adsorbates on the surface of the QD (5). These spectra are also used to find the concentration of QDs in solution and to quantify non-specific binding of ligands on QDs [10].

1.2.1 FRET

Another very important tool for characterizing QDs is Förster Resonance Energy Transfer (FRET). The basic model of FRET is based on an excitation energy non-radiative transfer that goes from an excited state donor (the QD) to an excited state acceptor (dye) [11]. The non-radiative energy transfer is a Columbic interaction from dipole-dipole coupling [12]. Figure 3 shows a schematic of the FRET phenomena works. An outside energy source, laser



energy, is used to excite the donor from a relaxed state to an excited state. At that point, it relaxes back down to the lowest excited state. The energy release from the donor when it returns to the ground state can promote the acceptor to an excited state. When the acceptor relaxes, there is an emission at its wavelength.

In order for FRET to occur, a few factors must be met. First, the donor needs to have a high quantum yield and both donor and acceptor spectra should be well resolved [13]. Also, the donor and acceptor must be within a certain proximity to each other; about 10 Å to 100 Å [14]. There must also be spectral overlap of the donor emission spectrum and the acceptor absorption spectrum (14). These conditions make QDs particularly useful for FRET studies. When compared to other fluorophores, such as organic dyes, QDs have high photostability, broad absorption spectra, narrow emission spectra, and these spectra are easily tunable by adjusting the QD size [15, 16]. A final condition for FRET to occur is the correct relative orientation and interaction between the two transition dipole moments. This parameter is given a quantitative value of κ^2 [17]. When the donor and acceptor dipoles are freely rotating the geometric average of this orientation

parameter has a value of $\kappa^2 = 2/3$ [18]. κ^2 can theoretically have values of 0 when dipoles are perpendicular to each other, 2 if they are parallel, and 4 when dipoles are collinear [19].

The efficiency of this energy transfer corresponds to the proximity of the donor to the acceptor. Specifically, the FRET efficiency (E) is dependent on the distance between the FRET pair (R) by the inverse sixth power [20]. This relationship is shown in Equation 1 [21].

$$E = R_0^6 / (R_0^6 + R^6) \quad \text{Equation 1}$$

The term R_0 is the Forster distance and is the point where there is 50% FRET efficiency [18]. This value can be calculated using κ^2 (the orientation factor between the two dipoles), the donor quantum yield (ϕ_d), the refractive index (n), and the spectral overlap integral (J_{da}) as shown in Equation 2 [21].

$$R_0^6 = (8.79 \times 10^{-25}) \kappa^2 n^{-4} \phi_d J_{da} \quad \text{Equation 2}$$

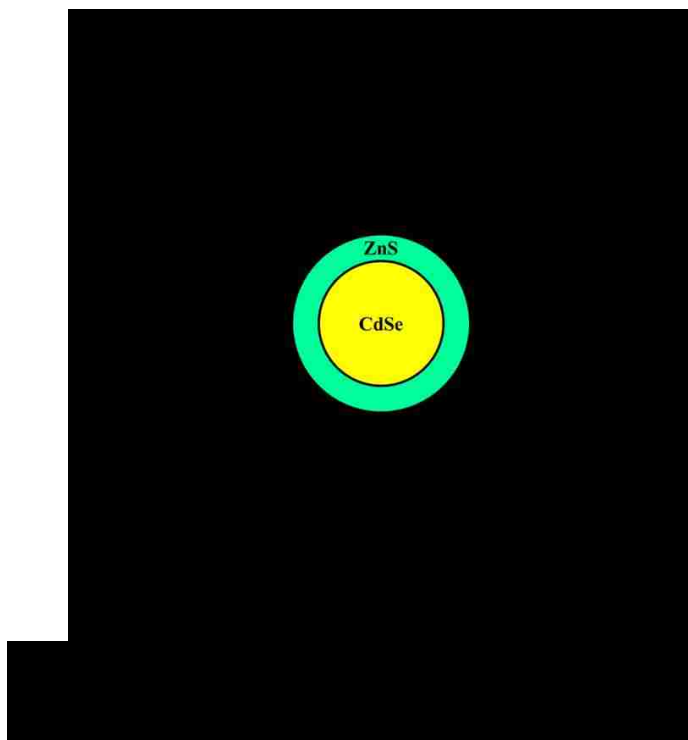
This information can be used to identify structural confirmation or even report on concentration [22]. FRET can be used at the ensemble and single particle level. The benefit of being able to use FRET for single molecules is that it allows for the observation of single molecule dynamics.

1.3 Quantum Dots: Development

The synthesis of quantum dots made a significant leap in the 1980s when Rossetti, Nakahara, and Brus reported on QDs created in solution, called colloidal quantum dots [23]. Colloidal QDs have become the foundation for a great deal of research that continues today. Predictably, the earliest work with colloidal QDs focused on their synthesis and basic characterization. By the early 1990s, the some of the characteristics that make QDs so useful were

being discovered. For instance, Murray, Norris, and Bawendi reported on how it is easily possible to select a desired range of sizes of QD by removing them from the synthesis reaction at certain time intervals [6]. Another major advancement was made in 1996 by Hines and Guyot-Sionnest. They highlighted the importance that QD surface properties have on their structural and optical properties. They added a shell onto a QD core that passivated the surface and greatly enhanced the optical properties and made the nanocrystals more structurally stable [7]. In the next couple of years, other research groups extensively characterized these core-shell QD to optimize their optical and structural properties [24]. These works resulted in the development of the core-shell CdSe-ZnS QDs that are used in the investigations in this thesis.

The next development on the long pathway leading to the applications of QD research was rendering the QD water soluble while maintaining fluorescence. This was accomplished by the end



of the 1990s. Chan and Nie rendered QDs water soluble by encapsulating them with mercaptopropionic acid, providing the basic schematic that I followed [25]. Figure 4 shows a

schematic of the core-shell CdSe-ZnS QD capped in mercaptopropionic acid ligands. The reason for creating water soluble QDs was rooted in a desire to use them in biological applications. Their optical properties make them great candidates for use in biological imaging and sensing. This was previously an application for organic dyes and genetically modified fluorescent proteins [26]. QDs have distinct advantages over other biological labeling techniques in that they have a combination of high absorption cross-sections and good quantum yields, are more resistant to photobleaching, and they have narrow emission spectra and wide excitation spectra [27, 28]. In addition, QDs are more resistant to photobleaching and have been shown to have longer fluorescence lifetimes for cell imaging than organic dyes [29].

Once the QDs were rendered water soluble using ligand exchange, it became important to understand these ligand interactions. This, literally and figuratively, added another layer to consider when studying structural and optical properties. The additional issue of ligand functionality also became an area for study. Preliminary work has already been performed that has led to better understandings for these topics. In 2001, Aldana, Wang, and Peng examined the photochemical instability of thiolated ligand coated QDs [30]. It was observed that photochemical oxidation of the ligands occurred before the QD. As a result, the ligands would form disulfide bonds on the surface of the QD which caused the QD to precipitate out of solution. However, this could be delayed by the presence of free thiol ligands in solution or if the disulfide ligands were insoluble in water. A 2007 report by Breus, Heyes, Nienhaus included a study of fluorescence quenching caused by thiolated ligands [31]. They determined that the size and charge of the ligand molecule affects the quenching efficiency, the smallest quenching the most. There has also been research conducted on synthesizing ligands and creating capping systems to create more stable or functional QDs. In 2007 a group worked to develop a capping system that created water soluble

QDs that were biocompatible, while at the same time reducing the instability that environmental factors like pH can cause [32]. They created a system that used a thiol “anchor” ligand connected to a poly(ethylene glycol) (PEG) that was created to have different functional groups on the end [32]. Finally, in 2013 a report from the Heyes group was published on how monodentate versus bidentate ligands effect non-specific binding on the surface of QDs by using thiolated dyes as sensitive reporters [33]. Due to previous research on the increased stability of bidentate ligands, it was a surprise that in low ratios of dyes to QD their ability to inhibit non-specific adsorption was worse. It is the possibility for additional discoveries such as this that make further research on the topic important.

1.4 Purpose

A common method of QD water solubilization and functionalization is coating the surface with thiolated ligands [34]. This practice is used in many applications of QD research. One such application used dihydrolipoic acid capped QDs to create nanoscale biosensors by forming hybrid inorganic-bioreceptor assemblies through binding QDs to Escherichia coli maltose-binding protein [35, 36]. Theses ligand capped QDs can also be used for labeling and tracking. For instance, thiolated ligand coated QDs were covalently attached to streptavidin and used for labeling and single particle tracking of the interaction of biotinylated epidermal growth factor (EFG) to EFG receptors of live cells [36, 37]. However, the QD surface interactions of these ligands are not fully understood. There has been previous work done to understand thermodynamic aspects of these interactions, but that is only part of the story. The binding kinetics that can be gathered from time based FRET measurements provides insight about the exchange mechanisms of target molecules bound to the QD surface.

In this investigation, modified fluorescent dyes are used to study exchange kinetics through quenching QD fluorescence upon binding to the surface. Water solubilizing thiolated ligands of different sizes, coordination geometry, and charges are exchanged with fluorescent dyes of different charges to study the effects this has on the exchange rate.

1.5 CdSe/ZnS Quantum Dots

The development and availability of commercial QDs has greatly increased in recent years. The increased applications result in there being a variety of structures and compositions to choose from. One of the most widely used of all nanoparticles is CdSe. This is due to the structural and optical properties that result from monocrystalline semiconductors composed of this material. Structurally, the size of CdSe QDs can range from 15 to 120 Å in diameter [38]. The optical advantages of CdSe are related to their absorption properties that result from their band gap energies. CdSe has a bulk bandgap of 1.7 eV, which means that its absorption energies can be tuned with particle size to cover the visible light region [39]. This makes them widely applicable to imaging processes.

CdSe nanoparticles alone have limitations. The CdSe cores are somewhat unstable because their small size results in a large surface-to-volume ratio that makes them highly reactive [40]. CdSe QDs also have optical deficiencies. Uncoordinated bonds at the outer edge result in surface states that are within the energy levels of the band gap, which can trap excited charge carriers [41, 42]. In order to optimize CdSe QDs they are commonly capped with a layer of ZnS, resulting in a core-shell structure. ZnS is used because it has a wider bandgap than the CdSe and therefore confines the electron and hole wave functions in the core [43]. The ZnS shell protects the core from environmental conditions and passivates the surface imperfections which leads to improved chemical and photostability, as well as higher photoluminescence quantum yields (QY) [24, 44].

The QDs obtained for this experiment are core-shell CdSe/ZnS (Figure 5). These QDs have a high photo luminescent intensity and a small size. The small size (<5 nm) corresponds to an ideal emission wavelength and less restrictive steric hindrance for future biological studies [33]. The fluorescence emission wavelength of the QDs used here is 520 nm, which ensures efficient spectral separation from the near-infrared dyes that are used as ligand reporters.

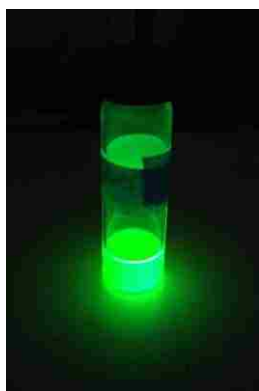
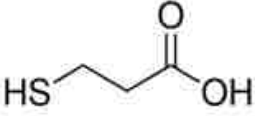
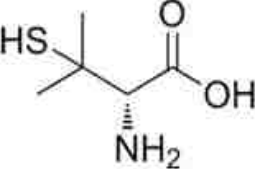
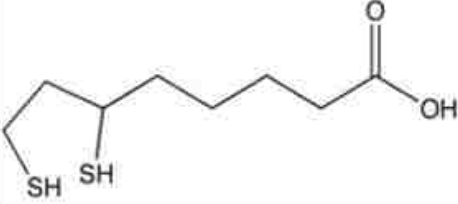


Figure 5: 520 nm CdSe/ZnS QDs in Toluene Under UV Lamp

1.6 Ligands

The ligands used to render QDs water soluble play an important role in their stabilization and functionality. They can vary in coordination, charge, and size. The three ligands used for this experiment were chosen to compare these varied properties. All of the ligands have a hydrophobic thiol group that will bind to the ZnS shell and a hydrophilic carboxylic acid end group that could be functionalized for later research [45]. They are mercaptopropionic acid (MPA), D-penicillamine (DPA), and dihydrolipoic acid (DHLA). Their structures and charges at physiological pH are compared in Table 1.

Ligand Name	Structure	Charges
3-Mercaptopropionic Acid		Negative
D-Penicillamine		Zwitterionic
Dihydrolipoic Acid		Negative

1.7 Fluorescent Dyes

The fluorescent dyes chosen for this experiment are both commercially available, water soluble, near-infrared, and functionalized with amine groups. Their primary difference is the overall charge each dye carries. ATTO 700 amine (ATTO) is a zwitterionic dye from Atto-Tec GMBH. This dye has a molecular weight of 836 g/mol, an absorption of 700 nm, an emission of 719 nm, and a molar absorbance of $120,000 \text{ M}^{-1} \text{ cm}^{-1}$ [46]. The second dye used is PromoFluor 700P amino-modified (PROMO) from PromoKine. PROMO has a molecular weight of 791.01 g/mol, and absorption of 706 nm, an emission of 731 nm, and a molar absorbance of $140,000 \text{ M}^{-1} \text{ cm}^{-1}$ [47]. In order for these dyes to bind to the QD surface and act as ligand reporters the amine groups are reacted with SATA (see below) to make modified thiolated dyes. Thiolated dyes are known to bind to the QD surface and compete with the already-bound thiolated ligands, although the kinetics of this exchange are not known [33].

1.7.1 SATA

The modification of the amine group of dye is accomplished using N-Succinimidyl S-Acetylthioacetate (SATA) (Figure 6). The N-hydroxysuccinimide forms an amide bond with the amine group on the dye. The thiol group is initially in protected form (thioester) and must be deprotected with hydroxylamine-HCl before it is used for binding to the QDs (Figure 7).

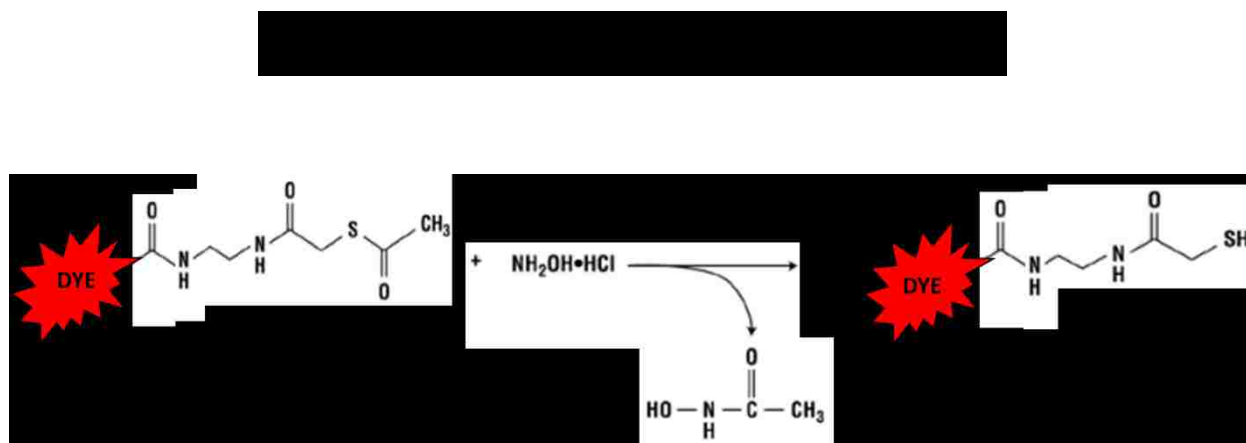
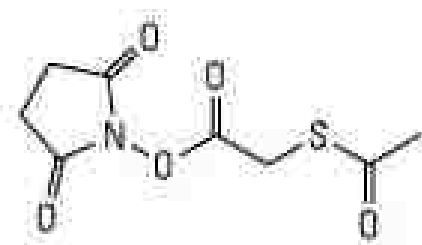


Figure 7: Deprotection of the SATA modified dye with hydroxylamine-HCl to expose the sulfhydryl group.

Chapter 2: Experimental Methods

2.1 Quantum Dot Characterization

For this project commercial QDs were obtained from Ocean Nanotech (San Diego, CA). These core/shell CdSe/ZnS QDs were coated with a native organic ligand octadecylamine (ODA). Upon arrival, the QDs were in a dried form and had been kept chilled. The ODA-QDs were made into solution by dissolving them in toluene. This sample was characterized by absorption and photoluminescence spectroscopy. The absorption was measured on a U-3900H Spectrophotometer (Hitachi) and the photoluminescence was measured using a LS 55 Luminescence Spectrophotometer (Perkin Elmer). The QDs have an absorption maximum of about 500 nm and emission maximum of 520 nm (Figure 2.1).

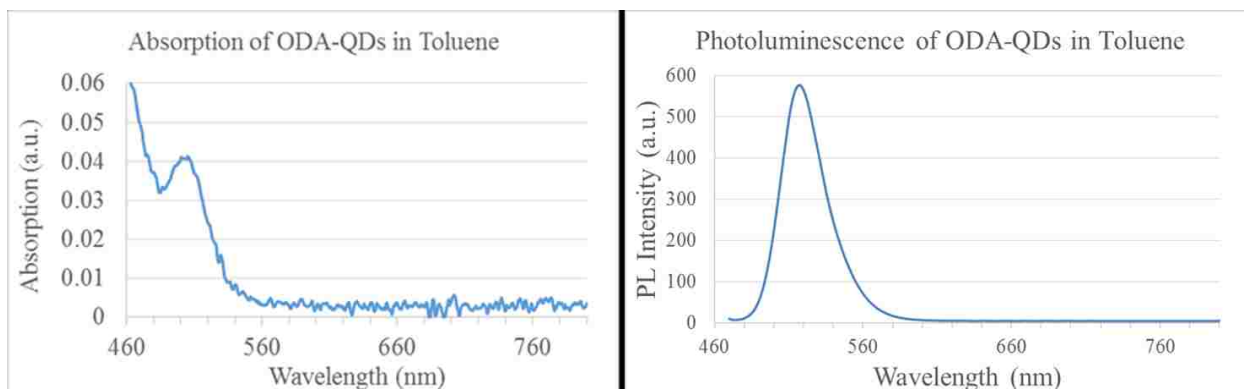


Figure 2.1: Absorption and Photoluminescence of CdSe/ZnS Quantum Dots in Toluene

2.2 Quantum Dot Purification

Acetone was used to precipitate the ODA-QDs out of the initial toluene solution. The solution was centrifuged first at 4,000 rpm on a VWR Clinical 50 for 15 minutes and the supernatant decanted from the pellet. The slightly fluorescent supernatant was then centrifuged at

14,500 rpm on a Centrifuge MiniSpin plus for 10 minutes. After this, the supernatant was discarded and the QD deposits were dried under Argon. In order to remove excess native ligands the QDs were dissolved in hexane and mixed with equal parts methanol. This was then centrifuged at 4,000 rpm for 15 minutes. The clear supernatant was checked for fluorescence and, if absent, was discarded. Finally, the QDs were re-dissolved in hexane and then washed a final time using acetone. This required centrifuging at 14,500 rpm for 15 minutes. The non-fluorescent supernatant was discarded and the resulting QD accumulation was dried with Argon in order to prevent oxidation.

2.3 Ligand Exchange and Phase Transfer

The purification process is the same for all ligands used. However, the process for performing the ligand exchanges varied slightly based on the ligand used. Each ligand exchange was performed using refluxing.



Figure 6.2: Ligand Exchange Reflux Apparatus

2.3.1 Mercaptopropionic Acid (MPA)

The ligand exchange solution was made using 5 mL of methanol in a 20 mL vial to which 0.00231 mol of the ligand (202 μ L of MPA (Alfa Aesar)) was added. The pH of the solution was adjusted to 10-11 by adding tetramethylammonium hydroxide pentahydrate (TMAOH) and,

checked using BDH pH test 0-14 strips. The ligand exchange was performed by dissolving the previously purified QDs into the ligand solution. The solution was transferred to a three-necked flask for refluxing (Figure 2.2). A Digi-Sense Temperature Controller was used to reflux the solution at 60 °C for 3 hours under Argon flow. The solution was then cooled to room temperature and centrifuged to remove unreacted product. Phase exchange was performed by precipitating the MPA-QDs out of solution using acetone and centrifuging. The QD deposit was dried under argon and then dissolved in Millipore water.

2.3.2 D-penicillamine (DPA)

For the DPA (Sigma) ligand exchange, 30 mL of 2-propanol was used as the solvent. DPA (80 mg) was added and mixed on a vortex mixer and then sonicated. The pH was then adjusted using TMAOH until it reached 12-13. The solution was again mixed until it became clear. The purified QDs were dissolved in the ligand solution and added to a three-neck flask. The solution was then refluxed at 70-80 °C for 20 minutes under Argon. The DPA-QDs were precipitated out of the ligand solution with ethyl acetate and centrifuged at 17,000 rpm for 45 minutes. The DPA-QDs were dried under argon and then dissolved in Millipore water.

2.3.3 Dihydrolipoic Acid (DHLA)

The DHLA used was reduced from the as-purchased (\pm)- α -Lipoic Acid (Sigma) by reaction with sodium borohydride (Alfa Aesar) and sodium bicarbonate (EMD) [48]. 3g of lipoic acid and 0.6g NaBH₄ were added to a 250 mL flask. 58 mL of 0.25 M NaHCO₃ was slowly added. The flask was placed in an ice bath and stirred for 30 minutes. Then 50 mL of toluene was added and the pH was adjusted to 1 using chilled 5 M HCl. This solution was stirred for 5 minutes and the

layers were allowed to separate. The toluene layer (top) was collected in a round bottom flask and rotovaped under high vacuum to remove the solvent.

The ligand solution included 5 mL of methanol and 0.00231 mols of the DHLA. The pH was adjusted to 10-11 with TMAOH. The solution was refluxed at 60 °C for 3 hours under Argon. The DHLA-QDs were precipitated out of the ligand solution with acetone. The DHLA-QDs were then dried under argon and dissolved in Millipore water.

2.4 QD-Ligand in Water Concentration

After each Dye-Ligand sample was dissolved in water, the concentration was calculated by measuring absorption spectra. The Lambert--Beer Law can be used to calculate the concentration of the QD solution using the absorption spectrum (Equation 2.1) [49].

$$A = cl\varepsilon \quad \text{Equation 2.1}$$

Where (A) is the absorption, (c) is concentration, (l) is the path length, and (ε) is the extinction coefficient. The extinction coefficient is size dependent and can be calculated using the wavelength of the absorption peak. The absorption value used for calculating concentration is a corrected absorption. The absorbance measured at the peak needs to be corrected for the size distribution of the particles that leads to the measured linewidth being larger than that of the homogenous linewidth. The absorption is calibrated when the size distribution of the QDs is broader than standard samples [50]. This correction is calculated by measuring the photoluminescence spectra. The corrected absorbance is found by (Equation 2.2) [50]:

$$\text{Corrected } A = (FWHM)(A)/K \quad \text{Equation 2.2}$$

FWHM is the full width at half the maximum of the PL peak, Figure 2.3. K is the homogeneous linewidth for the quantum dot species being used; for CdSe QDs it is 25 nm [50].

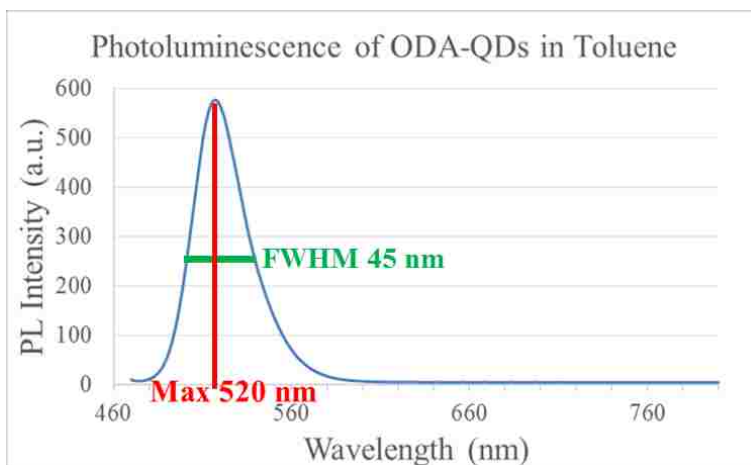


Figure 2.7: Full Width at Half Max Measurement

2.5 Dye Modification with SATA

The as-purchased dried dye powder was dissolved in 0.01 M PBS solution. For the dye modification, a small amount of this stock solution was taken and diluted for the experiment. The concentration of the dye in the stock solution was found by measuring the absorption at its λ_{\max} and dividing it by the molar absorbance ($120,000 \text{ M}^{-1}\text{cm}^{-1}$ for ATTO and $140,000 \text{ M}^{-1}\text{cm}^{-1}$ for PROMO). Following the published procedure for modifying the dye with SATA, the mole ratio of dye to SATA was set to 1:100 [51]. The SATA was weighed and dissolved in DMSO (55 mM solution). The SATA solution was then added to the dye and allowed to react in the dark at room temperature for 30 minutes. At this time, the deacetylation solution (hydroxylamine HCl, EDTA, and NaOH in PBS) was added to the Dye-SATA and allowed to react for 2 hours in the dark at room temperature. The absorbance of the final Dye-SATA was then taken and the final concentration calculated.

2.6 Dye Characterization

Previous work characterized the ATTO 700 SATA modification [51]. In order to verify the modification also works for PROMO 700, reverse-phase HPLC and MALDI-TOF mass spectrometry was used. A Shimadzu HPLC with an Eclipse XDB-C18 column was used to monitor the Promo 700 before modification and after modification with a dye:SATA mol ratio of 1:100. The less polar modified dye comes off the column later and the unmodified dye. The 1:100 ratio ensures that all of the Promo700 is modified. The MALDI-TOF mass spectra was taken on a Bruker Ultraflex II Mass Spectrometer. The absorption and photoluminescence spectra were also used to characterize the dye. This was done to ensure that the absorption and PL peaks did not overlap those of the QDs. Also, the absorption spectra was used to calculate the dye concentrations.

2.7 Fluorescence

The fluorescence data was collected using a Photon Technology International (PTI) Spectrofluorometer and the Felix GX Version 3 software. The program's time based acquisition setting was used. The excitation and emission were set to 480 nm and 520 nm, respectively to monitor the QD emission intensity as a function of time. The data collection was set to 5 points/sec with a duration of 5760 seconds (1.5 hours plus 5 minutes for initial QD measurement and 1 minute for adding and mixing dye). The volume of QD-ligand solution obtained from each phase transfer was divided among four sample vials and the total mols was calculated. QD:Dye mole ratios that were used in the experiment included 1:0.5, 1:1, 1:2, and 1:3. The mols of Dye-SATA need per sample were then calculated based on these ratios and the calculated QD-ligand concentration in the vials. If necessary, water was added to each of the QD-ligand solution samples to have a total volume of 450 uL to fill the cuvette enough to cover the instrument window.

Each sample was measured for approximately 300 seconds before adding the dye to obtain a stable baseline. After 300 seconds the instrument hatch was quickly opened and the



Figure 2.4: PTI Spectrofluorometer with top opening sample chamber hatch

dye was added and mixed via pipette (Figure 2.4). The hatch was then closed and the measurement continued for the duration of the 5760 seconds. At the end of each measurement, the samples were observed for any visual signs of aggregation or changes and were photographed. The prepared QD samples that were awaiting measurement and the dye stock aliquots were stored in the refrigerator until 30 minutes prior to being measured. This time allowed them to reach room temperature before measurement.

Chapter 3: Results and Discussion

3.1 Characterization of PROMO 700

The results of characterization of the reaction of PromoFluor700 to SATA show that the modification from amine to thiol functionality is successful. Figure 3.1 shows the reverse-phase HPLC data before and after modification. The conversion from amine to thiol makes the dye less polar and elutes of the column later. The MALDI-TOF mass spectra is shown in Figure 3.2. The increase in mass shown in the peaks after modification corresponds to the addition of SATA. They also include the addition of free Sodium ions from the dye solution. The absorption and PL taken after modification show that there is no significant change in the spectra from the thiolation modification (Figure 3.3).

3.2 Atto 700

The fluorescence data collected was graphed using Origin 8. Figures 3.4-3.6 show the complete set of data including the first ~300 seconds of recording only the QD signal and the 5670 seconds after the addition of the Atto 700. After the introduction of the dye, the fluorescence is immediately decreased. This indicates that some of the free thiolated Atto 700 dyes immediately binds to the QD surface and quench the fluorescence during the mixing time of the solution. The Atto 700 dye steadily continued to bind to the QDs, leading to a further decrease in the QD fluorescence, which then saturated at a level depending on the QD:dye ratio used. It was observed from the graphs that there appeared to be three time components; a very fast component occurring during the ~3 second mixing time, followed by a component of a few hundred seconds and a very slow component on the thousands of seconds timescale. This was verified by fitting the data globally to a tri-exponential decay functions (Equation 3.1) (Figures 3.7-3.9).

$$y = A_1 e^{\frac{-x}{t_1}} + A_2 e^{\frac{-x}{t_2}} + A_3 e^{\frac{-x}{t_3}} + y_0 \quad \text{Equation 3.1}$$

These time components are shown to fit a common mechanism for all four ratios of dye by utilizing a global fit on all four sets of data. This was the case for all three ligands used, although the values of the exact lifetime components varied from ligand-to-ligand. A second-exponential fit was attempted, however the residuals for those fits showed that the initial < 3 second component was not being included in the overall fit. The tri-exponential global fit data for all three ligands is listed in Table 3.1.

The percent amplitude for each component and the average lifetimes for each ligand are shown in Figures 3.10-3.12. For DHLA (3.12) it is easy to see a large percentage of fluorescence decrease in the first component (< 3 sec). This supports a mechanism proposed by Takeuchi, Omogo, and Heyes where the low surface packing density of the bent bidentate ligand leaves vacant spaces where dyes can bind without having to exchange with the native ligands [52]. The percent amplitudes of the second and third component remain generally close, however they differ very much in their time frames. There is an approximate decrease of about 14% over a period of about 300 seconds and a decrease of about 18% over more than 200,000 seconds. In the second component exchange the bound ligands are being exchanged with the dye reporters. After this exchange, the QD fluorescence is nearing a point of being quenched by FRET with the bound dyes. The FRET efficiency as a function of dyes attached per quantum dot has been shown to saturate at about 2-3 dyes [52]. After this second component exchange has occurred, the large dyes bound to the quantum dot could cause steric hindrance that prevents ligands from falling off and from more dyes attaching. In addition, there are also now free ligands in the solution that can

re-adsorb to the QD, competing with and slowing down additional dye attachment. Over the much longer time frame in the third component, we see this additional binding.

The percent amplitude for each component and average lifetime are graphed in Figure 3.10. The amplitude of the first very fast component of the MPA is less than that of the DHLA. This indicates that the geometry of the MPA does indeed allow the ligands to be closer packed on the surface, somewhat inhibiting the immediate binding of dyes to the QD surface. However, the largest percentage of fluorescence is still quenched during this component, so there are clearly still vacant sites on the surface where the dyes can bind without having to exchange the bound ligands. The percentage of binding in this first component steadily increases with increasing concentrations of the dye, suggesting that we are not at saturating levels of vacant binding sites on the QD. For the MPA, the second component amplitudes (A_2) have the smallest percentages out of all the ligands (which also increase with concentration). Correspondingly, it also has the shortest t_2 . Again, in support the previous findings, it is possible that as a result of the close packing on the surface multiple ligands must be displaced before a dye can bind due to the large size difference between MPA and the dye. This could also be the reason for a decreased level of binding in the second component. The third component for MPA has large amplitudes compared to DPA and DHLA. The process of the initial MPA ligands detaching from the surface and dyes binding may be conducive to initiating more ligands to leave the surface of the QD, although there is a significant delay in this process – possibly due to ligands rearranging on the surface as postulated in the Takeuchi, Omogo, and Heyes study. The amplitude of this later component decreases steadily with increased dye concentration. This makes sense with the steady increase that is seen in the first two components where there were more dyes binding with increased dye concentration.

The lower ratios are already close to being saturated with dyes from the first two components, however the higher ratios are not and can have greater binding in the third component.

The DPA is unique in the ligands in that it is the only zwitterion and experimentally in that the percent amplitude for the first and second components are actually rather similar. If following the previous two outlines, the first component is a result of immediate binding that is taking place without ligand exchange occurring. This component represents about 30-50% of the total decrease in fluorescence (Figure 3.11). Interestingly though, the second component is also in the same range with 40-60% of the total decrease in fluorescence. This ligand has the largest amount for the second component out of all three of the ligands. However, converse to MPA, it also has the longest second component time. Based only on the fact that it is monodentate, it would be expected to have similar results to that of the MPA. This is not the case for the second “first exchange” component. The increased amount of exchange occurring for this ligand may suggest that this exchange is being aided by the dye itself. The MPA and DHLA both have a single negative charge. This charge could be attracted or repulsed with the positive or negative charge on the dye, respectively. Since the DPA is zwitterionic, these interactions could be doubled. Unfortunately the structure of the Atto700 is not published so the relative positions of the charges are unknown. At this time, it is not unrealistic to suppose that the alignment of zwitterions from the ligand and from the dye could be causing this increased second component exchange. Like the DHLA, more binding during the first two components decreases the amount of binding that can occur in the much slower last component for the same reasons. It is still observable over the long time frame though.

3.3 PromoFluor 700

The above proposed mechanism was tested by varying the charge on the dye. However, when repeating the experiment with the negatively charged dye, PromoFluor 700, there was unexpected aggregation in all of the samples. This was visible in the cuvettes after the completion of 5760 seconds and appears as large fluctuations in the fluorescence intensity throughout the measurement. Figures 3.13-3.15 show the complete set of data including the first ~300 seconds of recording only the QD signal and the 5670 seconds after the addition of the PromoFluor 700. The fluorescence intensity does decrease with the initial addition of the dye. This decrease is smaller for with the PROMO than with the ATTO. The normalized intensities are shown in Figures 3.16-3.18. The fluctuations and aggregation of the sample was observed again after repeating the experiment. Photographs taken after the measurements of ATTO and PROMO samples can be seen in Figure 1. For the MPA, there was extreme and sudden aggregation for the two higher dye concentration ratios. The 1:2 ratios of the MPA-ATTO and MPA-PROMO are shown in the first column of Figure 3.19. The QD-Dye deposit is clearly seen at the bottom of the cuvette. For the DPA, it was the two lowest dye concentration ratios that displayed the most fluctuation in signal and resulted in aggregation of the samples. The ratio of 1:1 for both ATTO and PROMO are shown in the second column of Figure 3.19. The DHLA also showed large fluctuations for the smaller ratios. Particularly in the 1:1 ratio that is shown in Figure 3.16. For the lower ratios of MPA and higher ratios of DPA and DHLA, there was some binding similar to that of the ATTO. There is an initial fast component and longer slower components. However, in all cases there was some increases in fluorescence and fluctuations in the slower component that could perhaps indicate that dyes are falling off after binding to the QD surface. After re-evaluation

of the PromoFluor 700 manual, it is possible that the aggregation in this experiment is due to an issue with the solubility of the dye.

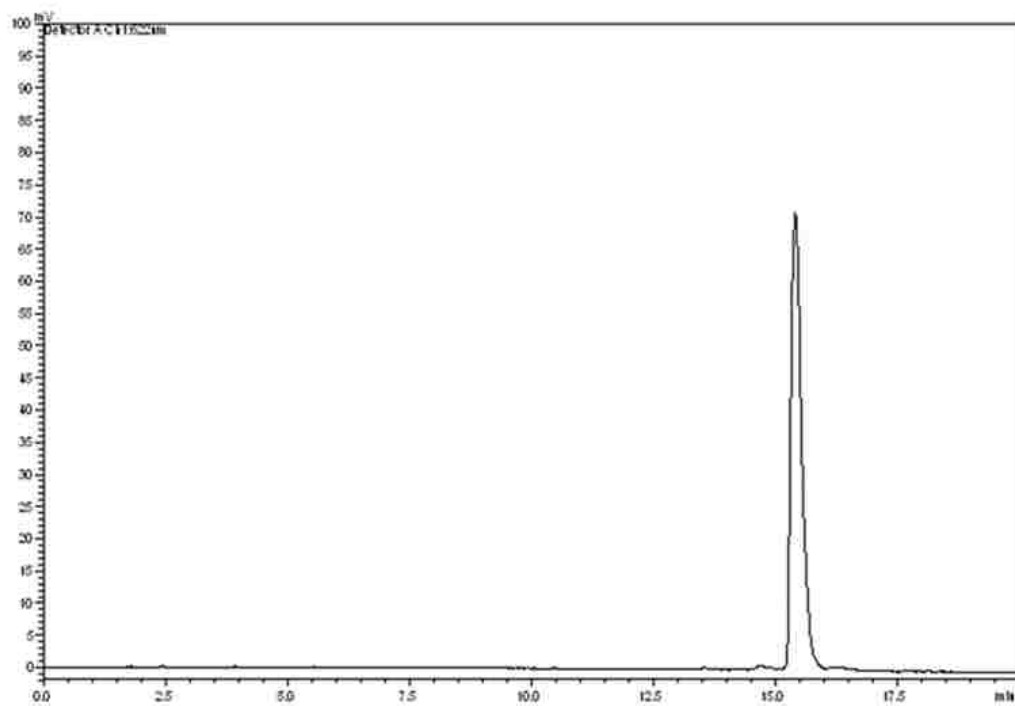
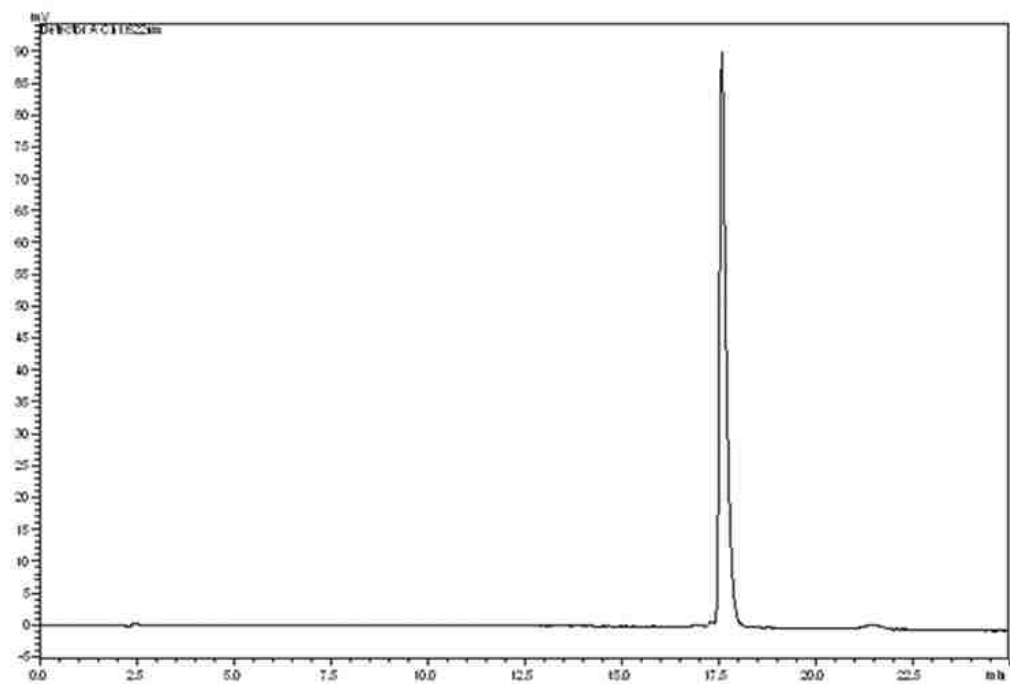
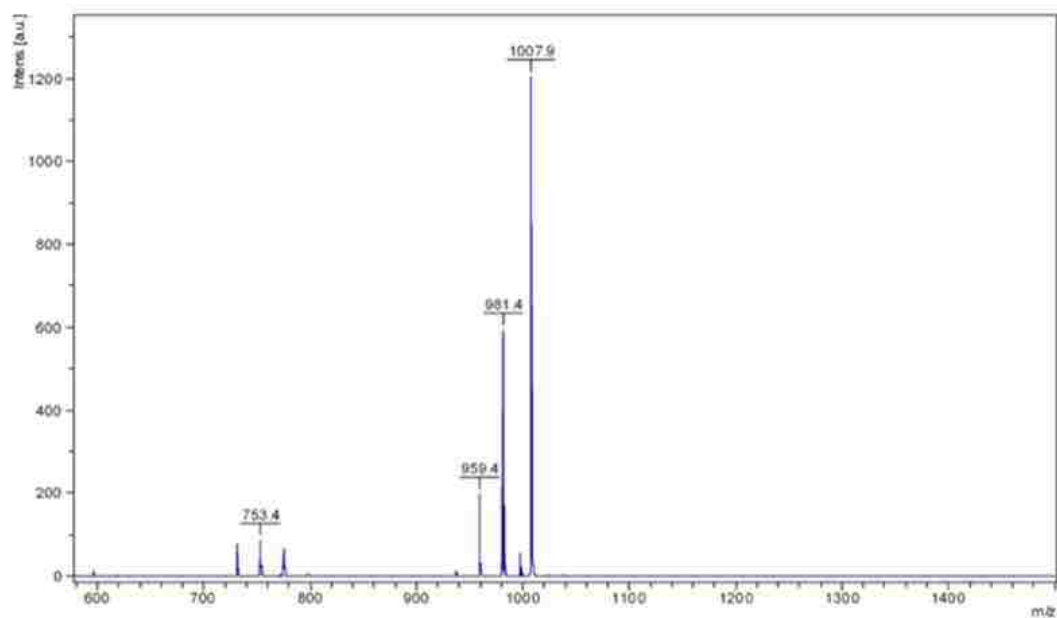


Figure 3.1: HPLC of PromoFluor 700 before and after modification with SATA., dye:SATA ratio of 1:100.

Sample Name : SATA-modified fluor 700

Sample ID# : 981677

Instrument: ultraflex II TOF/TOF



Arkansas Statewide Mass Spectrometry Facility
MALDI-TOF Mass Spectrum

Sample Name : Promo Fluor 700 RJM

Sample ID# : 981678

Instrument: ultraflex II TOF/TOF

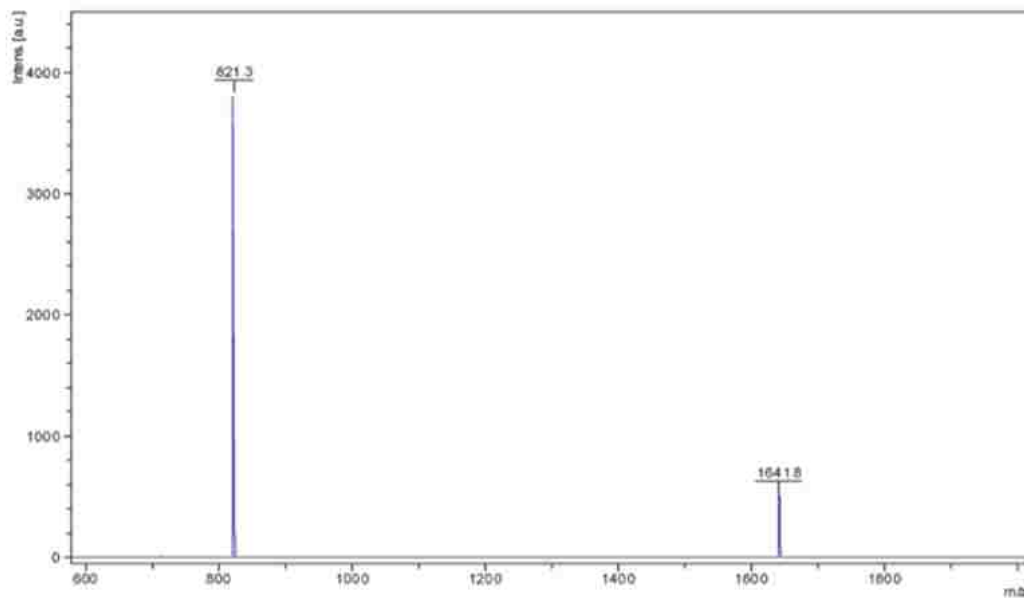


Figure 3.2: MALDI-TOF MS of PromoFluor 700 before and after modification with SATA.

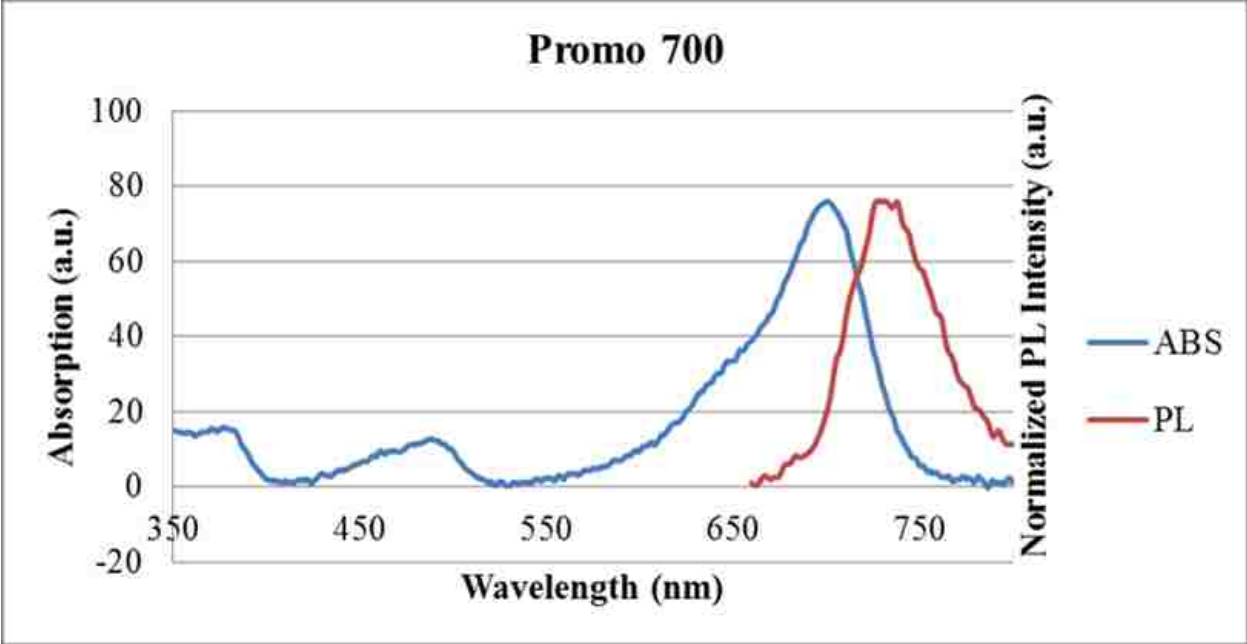


Figure 3.3: Absorption and PL spectra of PromoFluor 700 after reaction with SATA.

MPA ATTO

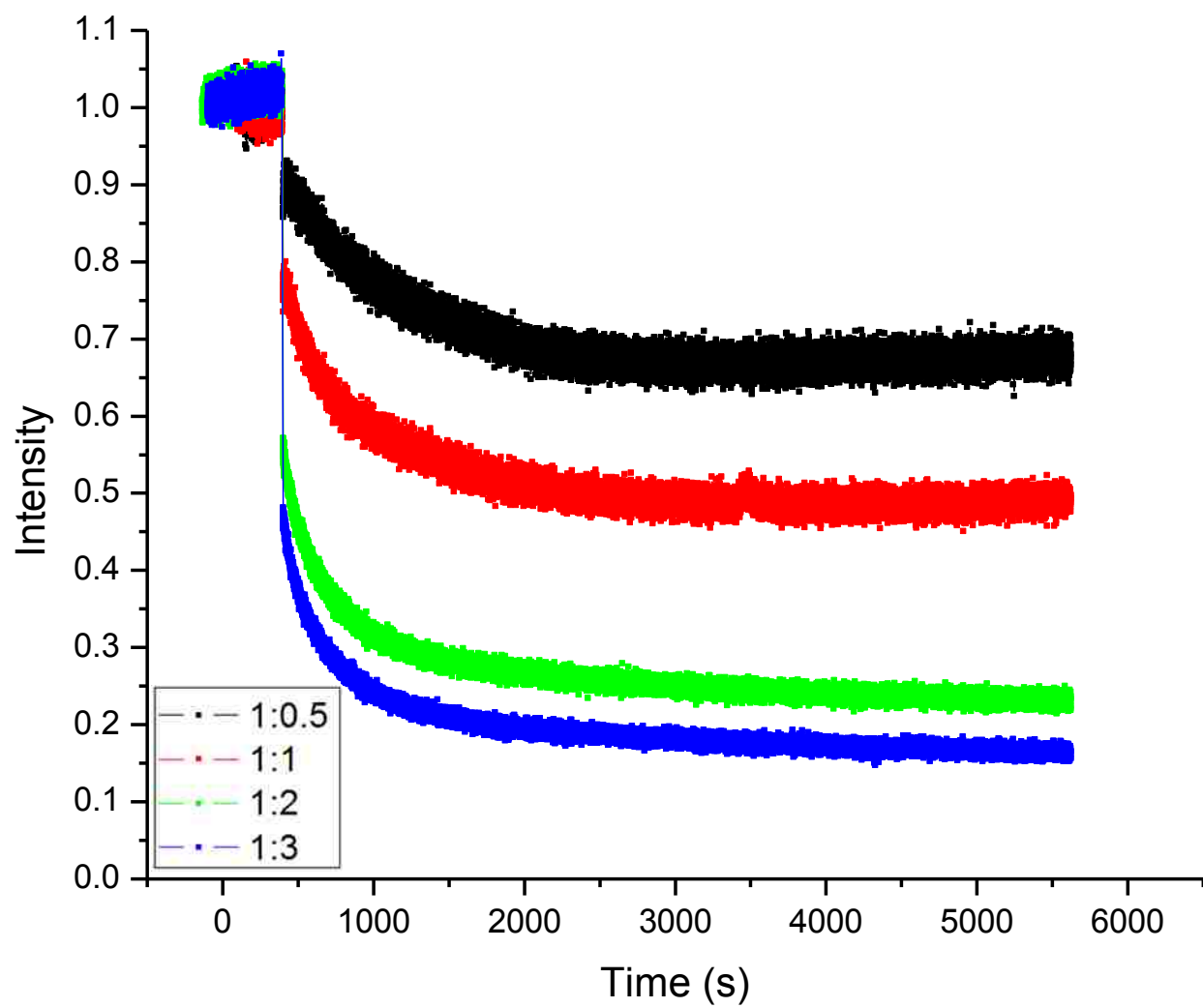


Figure 3.4: MPA-ATTO spectrofluorometer data.

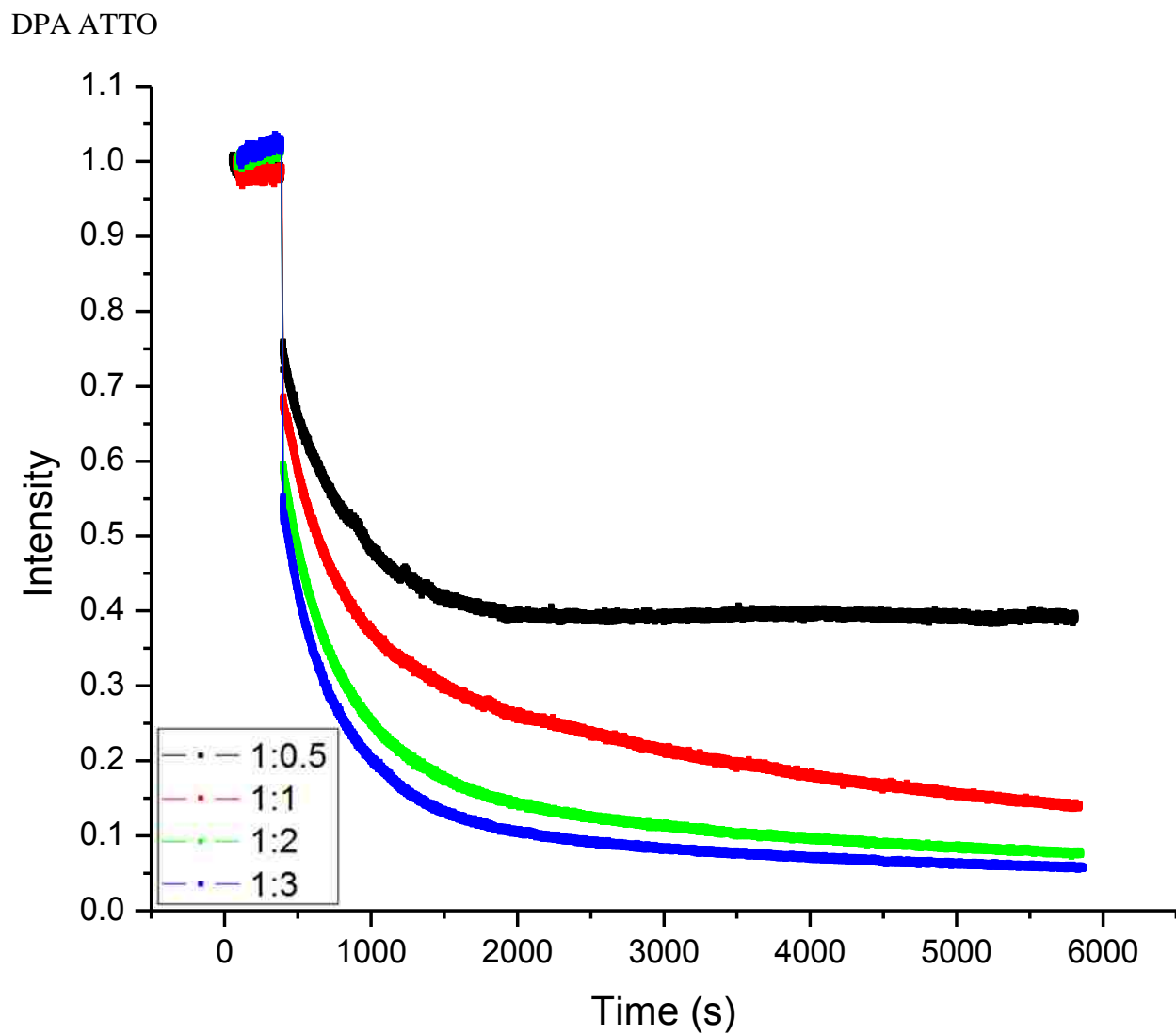


Figure 3.5: DPA-ATTO spectrofluorometer data.

DHLA ATTO

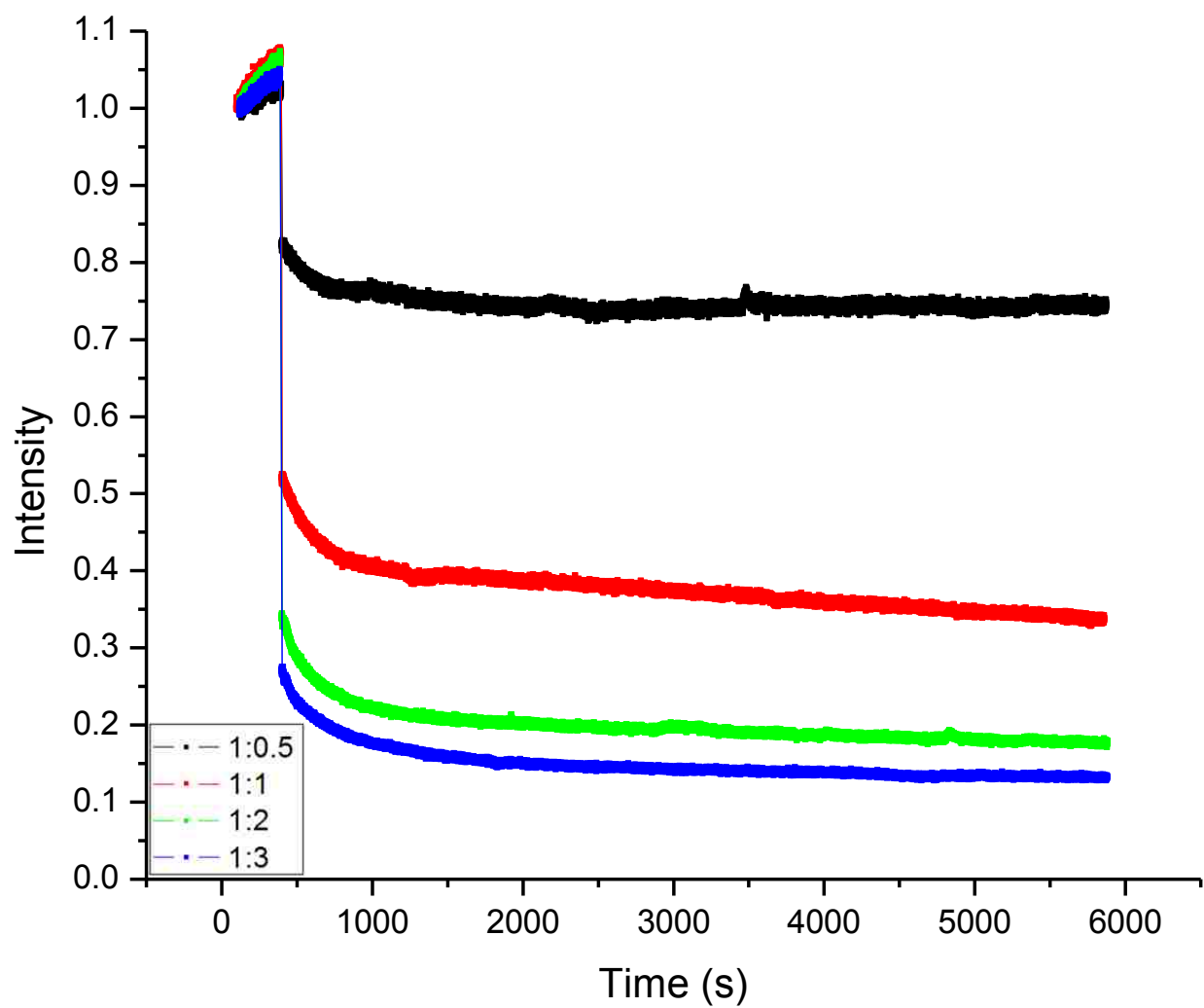


Figure 3.6: DHLA-ATTO spectrofluorometer data.

MPA ATTO

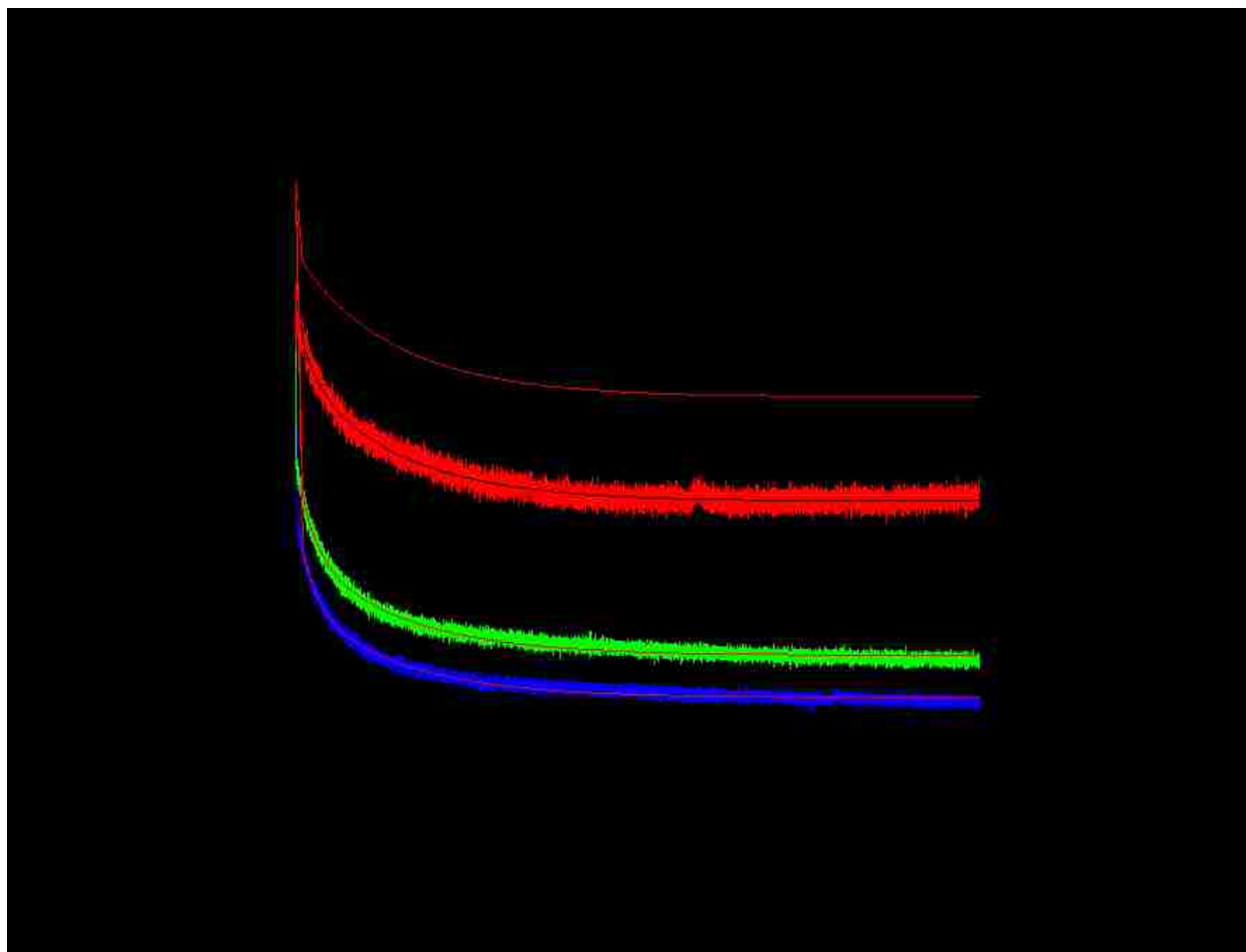


Figure 3.7: MPA-ATTO normalized spectrofluorometer data.

DPA ATTO

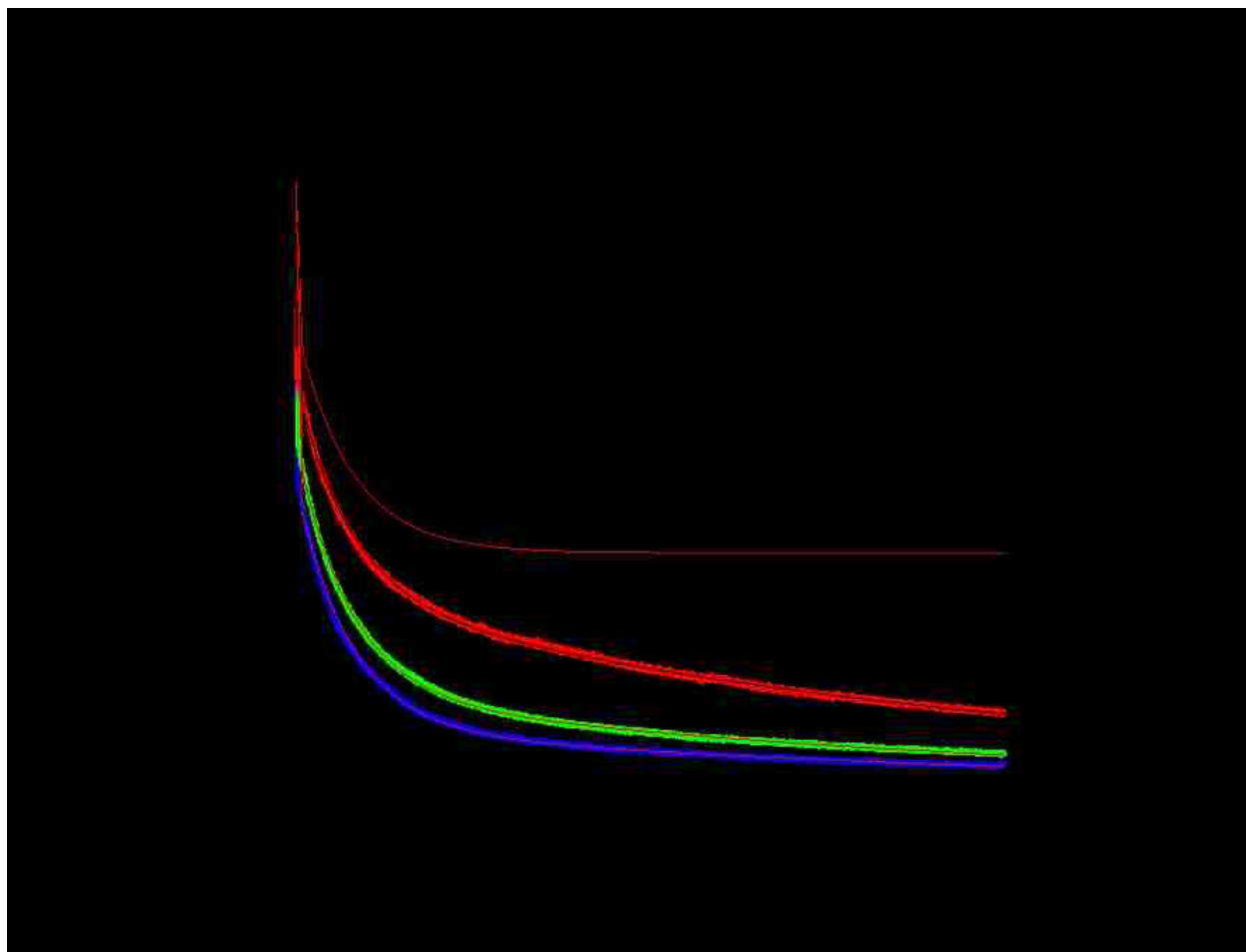


Figure 3.8: DPA-ATTO normalized spectrofluorometer data.

DHLA ATTO

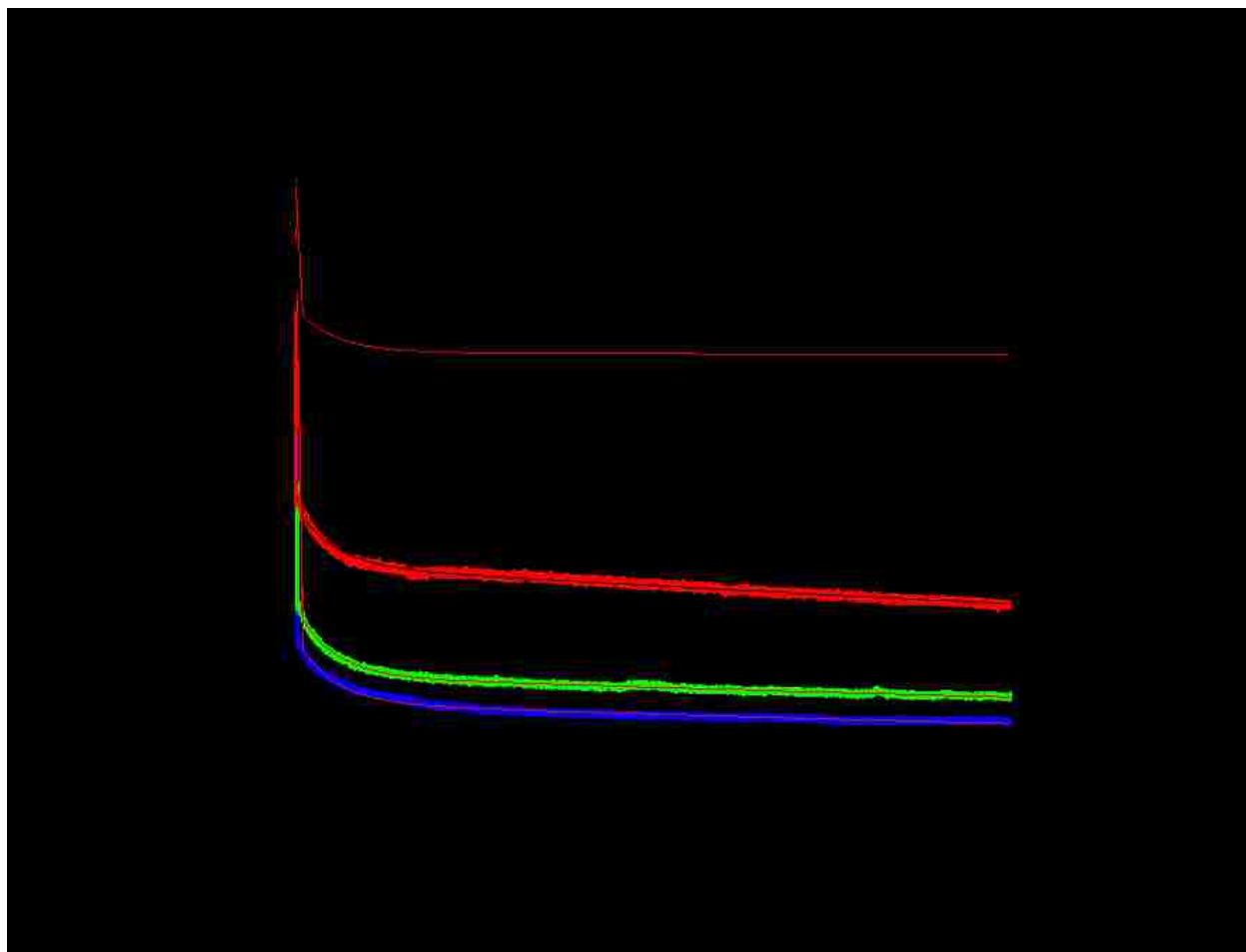


Figure 3.9: DHLA-ATTO normalized spectrofluorometer data.

MPA				DPA				DHLA			
t_1		0.15767		t_1		3.00000		t_1		2.63628	
t_2		128.52306		t_2		411.20835		t_2		283.93583	
t_3		764.87234		t_3		5028.64955		t_3		222868.33575	
1:0.5	Y_0	0.65016	%	1:0.5	Y_0	0.39598	%	1:0.5	Y_0	0.00000	%
	A_1	0.10720	31.1		A_1	0.22827	38		A_1	0.73848	73.8
	A_2	0.01097	3.2		A_2	0.36689	61		A_2	0.10589	10.6
	A_3	0.22639	65.7		A_3	0.00570	1		A_3	0.15566	15.6
1:1	Y_0	0.48163	%	1:1	Y_0	0.03725	%	1:1	Y_0	0.03933	%
	A_1	0.21165	41.1		A_1	0.31948	33.3		A_1	0.69084	71.8
	A_2	0.09176	17.8		A_2	0.33885	35.4		A_2	0.11093	11.5
	A_3	0.21177	41.1		A_3	0.30025	31.3		A_3	0.16016	16.7
1:2	Y_0	0.23277	%	1:2	Y_0	0.02120	%	1:2	Y_0	0.08716	%
	A_1	0.45345	59		A_1	0.42279	43.1		A_1	0.52380	57.6
	A_2	0.14070	18.3		A_2	0.40428	41.3		A_2	0.09359	10.3
	A_3	0.17463	22.7		A_3	0.15277	15.6		A_3	0.29135	32.1
1:3	Y_0	0.16463	%	1:3	Y_0	0.02132	%	1:3	Y_0	0.70213	%
	A_1	0.53977	64.6		A_1	0.49137	50.1		A_1	0.19699	67.7
	A_2	0.14015	16.8		A_2	0.39065	39.8		A_2	0.07332	25.2
	A_3	0.15552	18.6		A_3	0.09908	10.1		A_3	0.02080	7.1
$R^2 = 0.99793$				$R^2 = 0.99943$				$R^2 = 0.99975$			

Table 3.1: Global fit data for MPA, DPA and DHLA with ATTO.

MPA

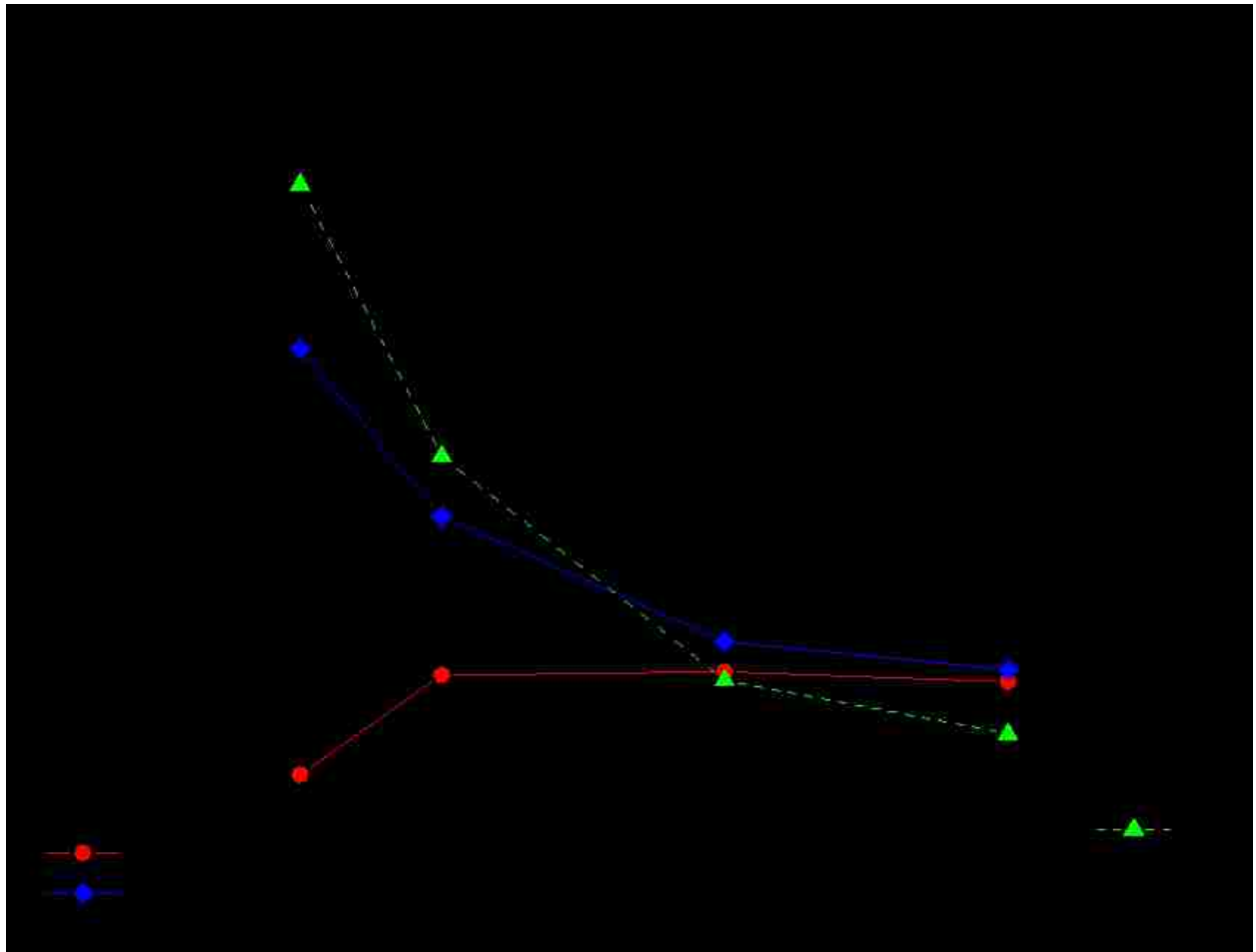


Figure 3.10: MPA percent amplitude and average lifetime.

DPA

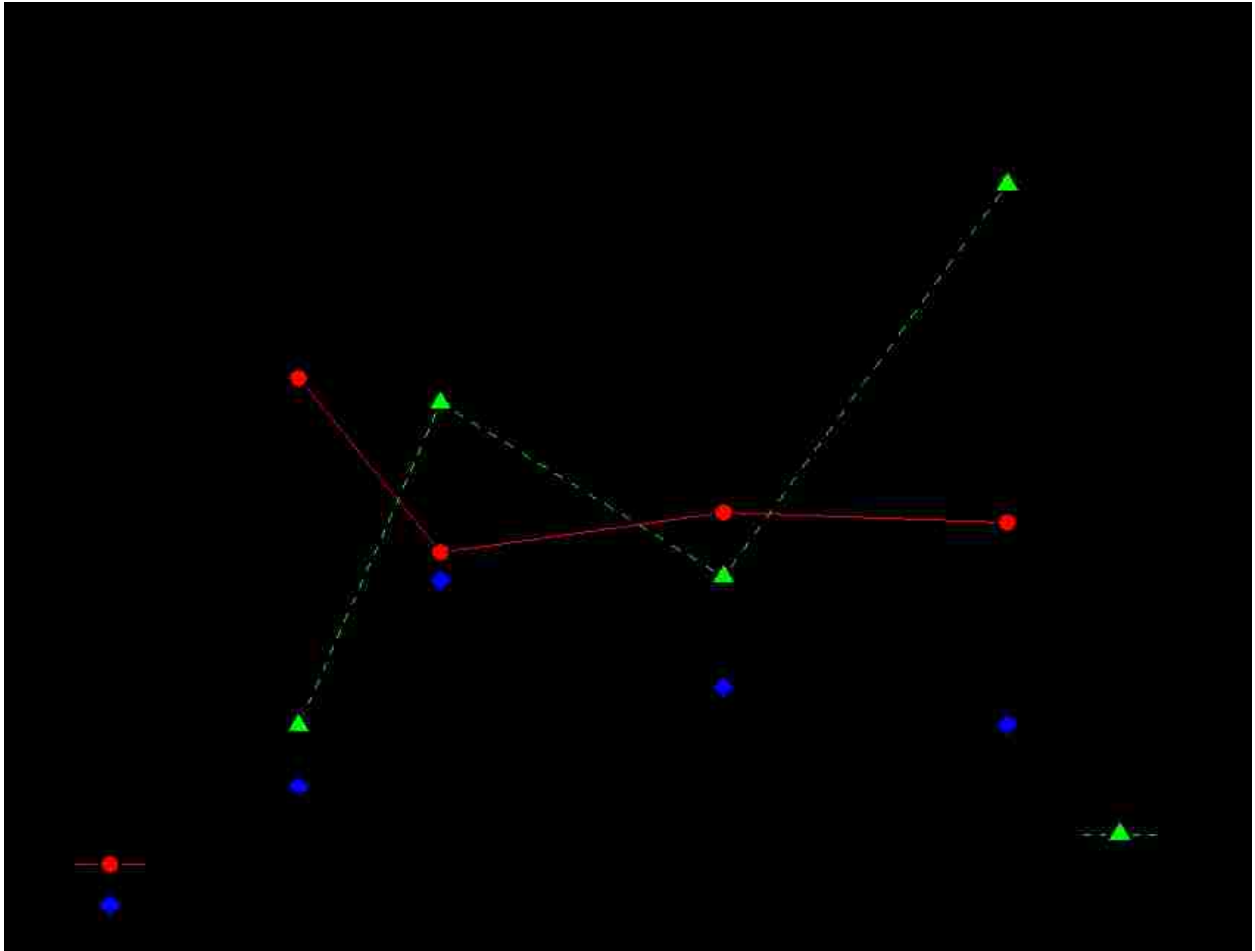


Figure 3.11: DPA percent amplitudes and average lifetime.

DHLA

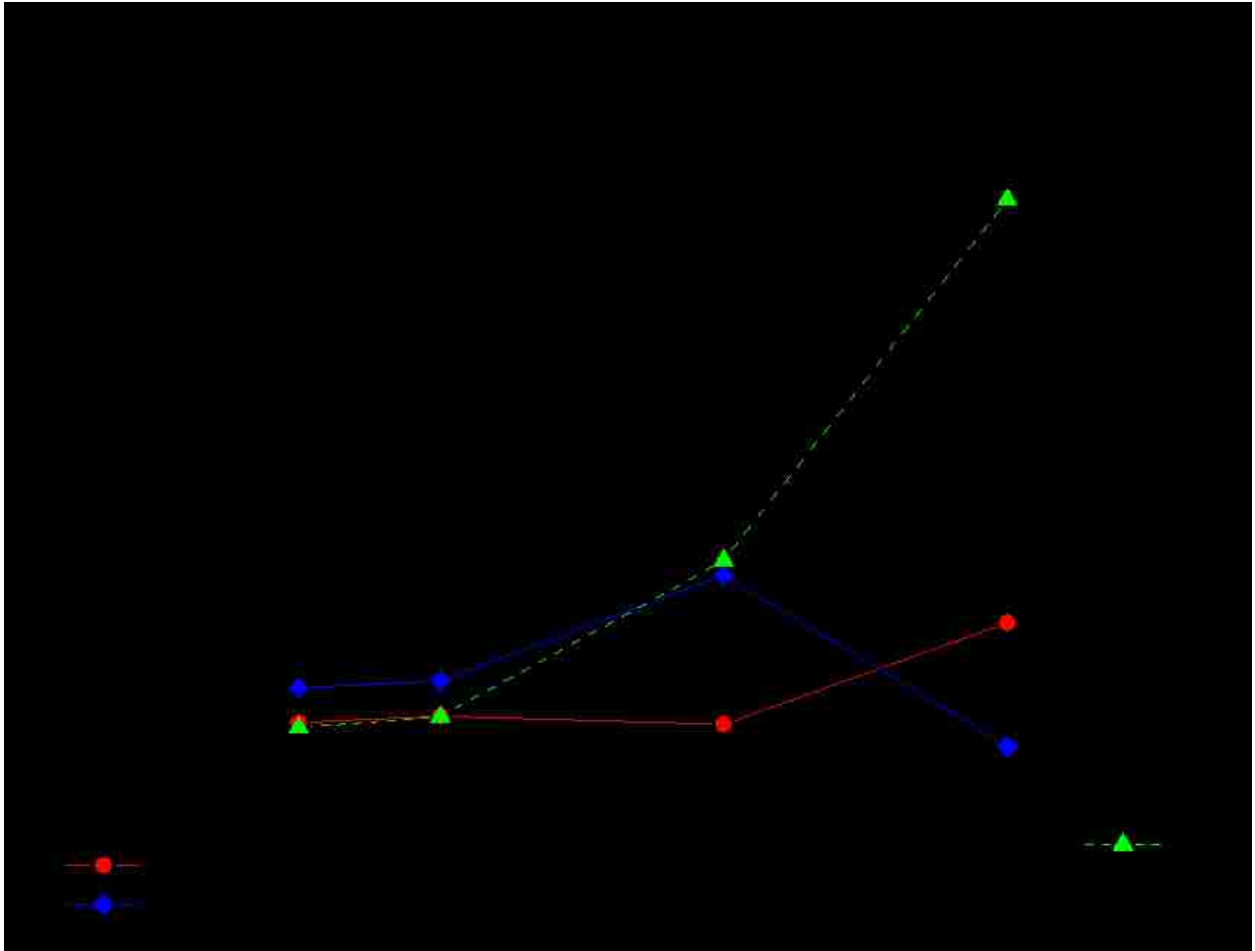


Figure 3.12: DHLA percent amplitudes and average lifetime.

MPA PROMO

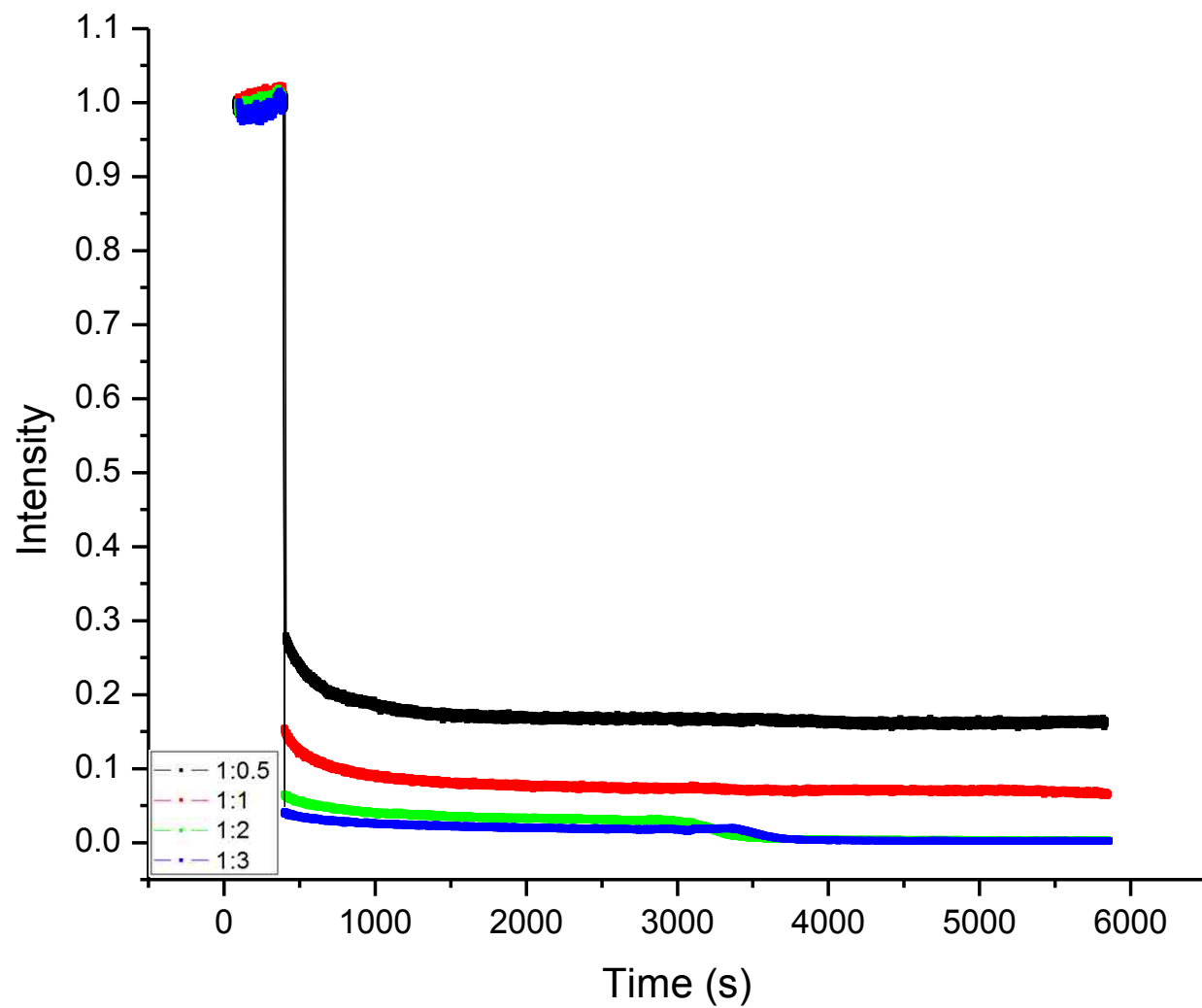


Figure 3.13: MPA-PROMO spectrofluorometer data.

DPA PROMO

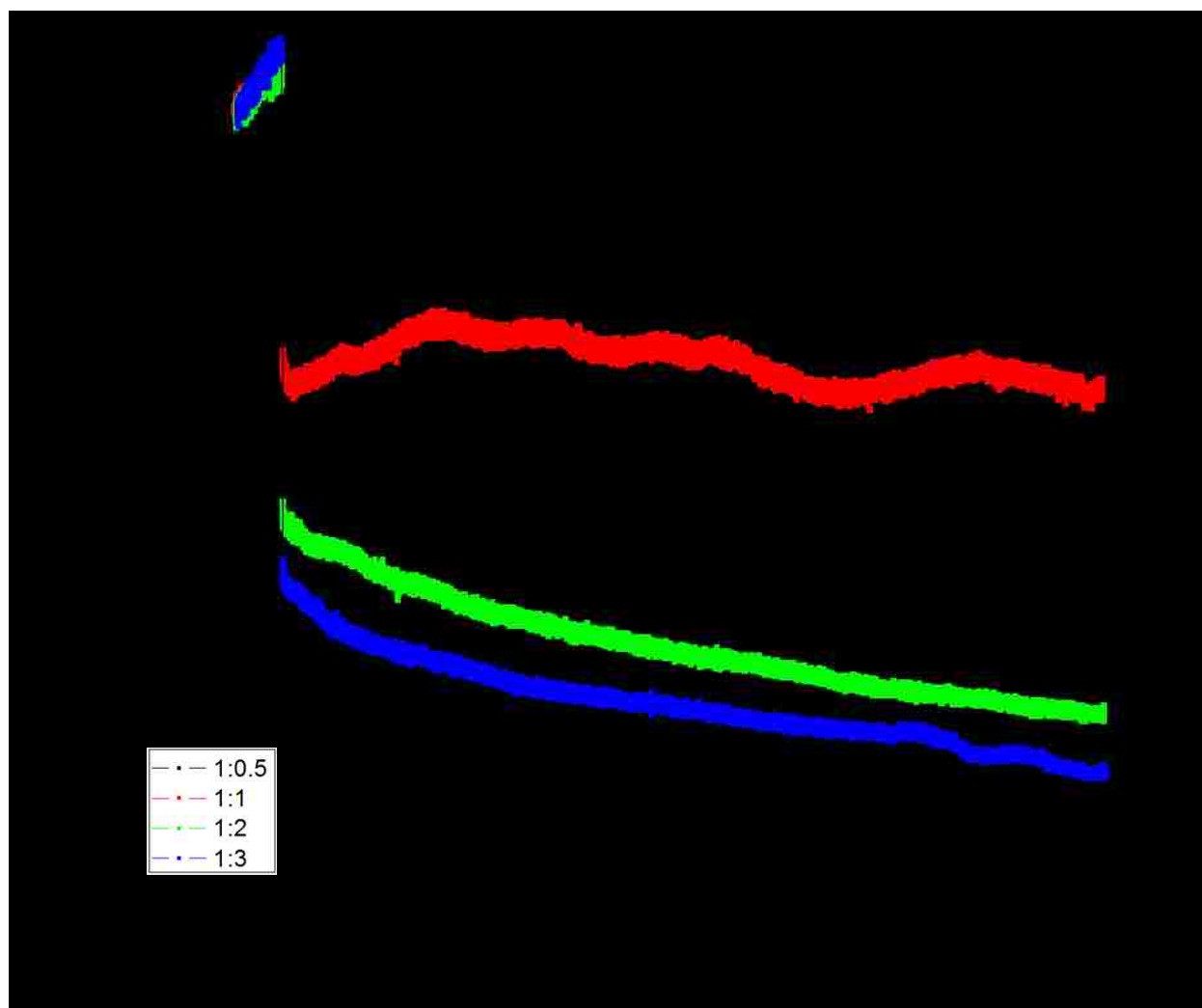


Figure 3.14: DPA-PROMO spectrofluorometer data.

DHLA PROMO

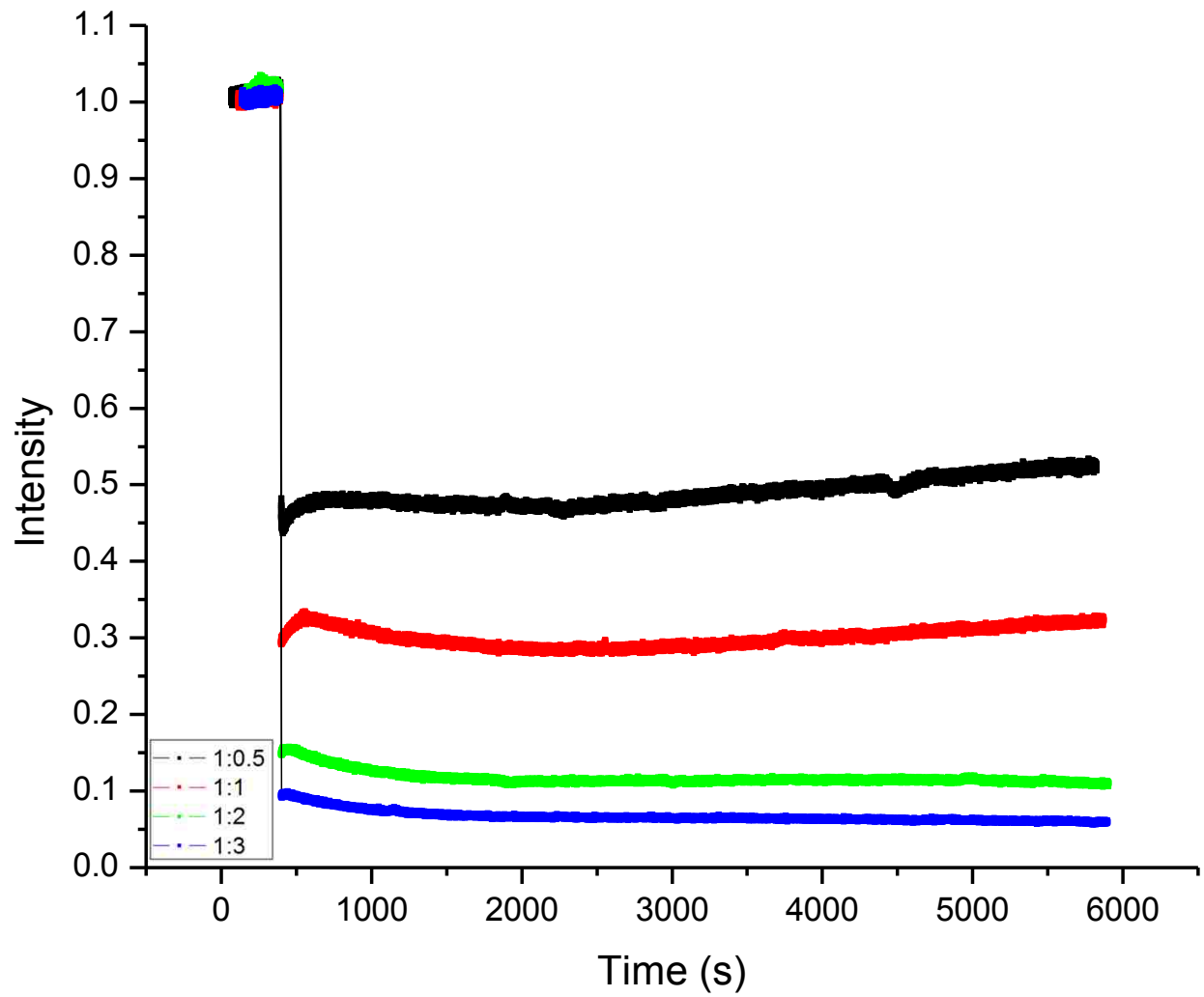


Figure 3.15: DHLA-PROMO spectrofluorometer data.

MPA PROMO

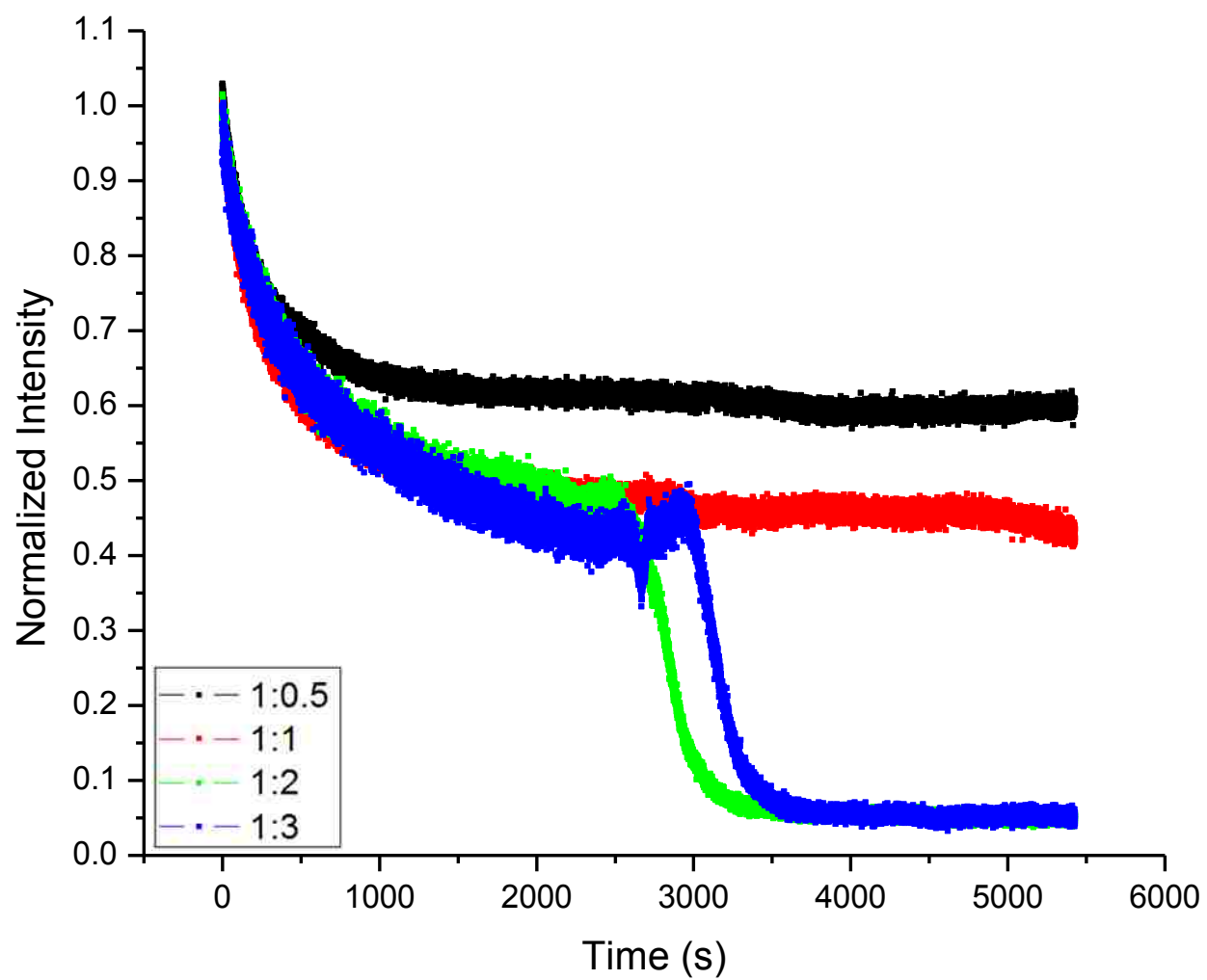


Figure 3.16: MPA-PROMO normalized spectrofluorometer data.

DPA PROMO

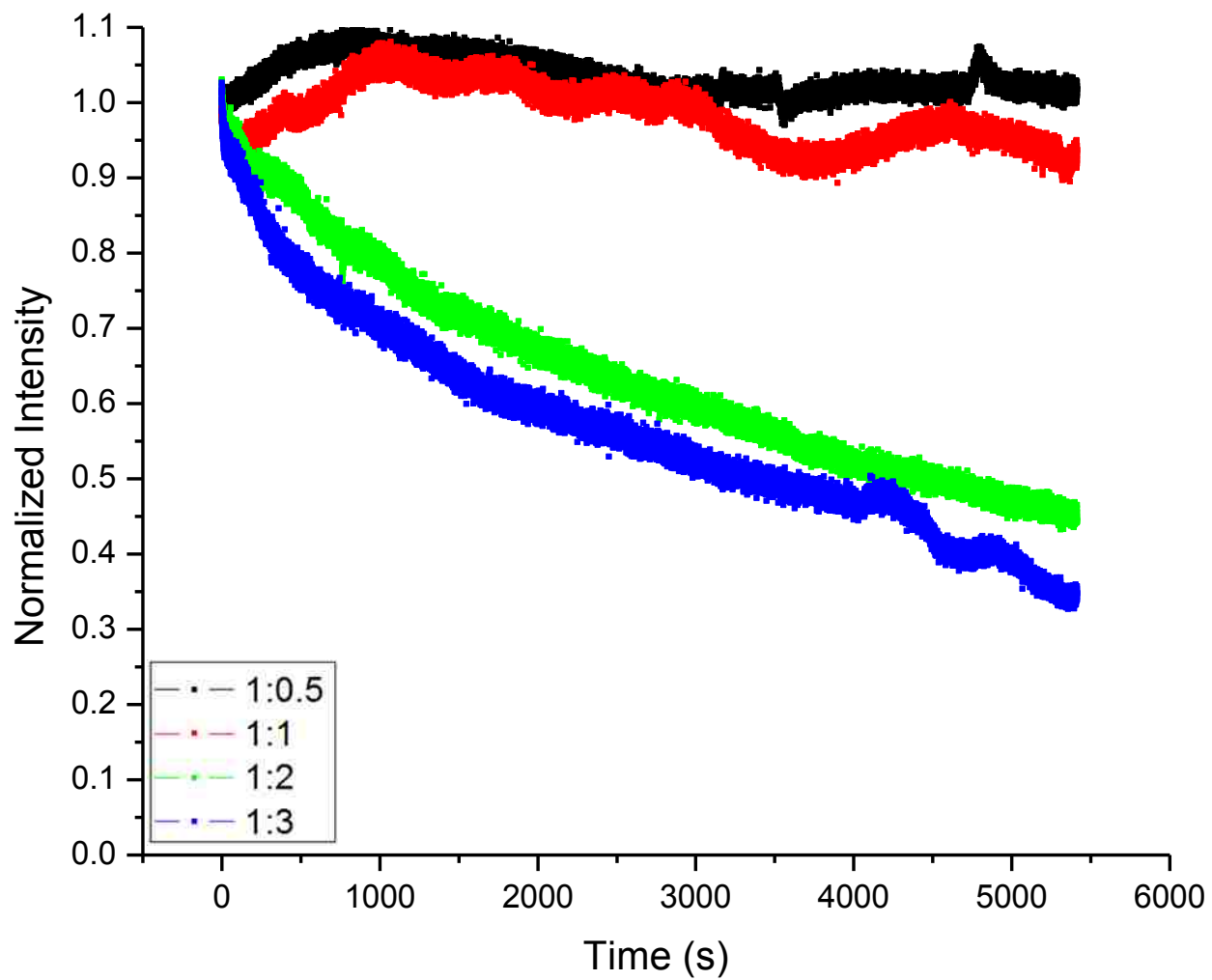


Figure 3.17: DPA-PROMO normalized spectrofluorometer data.

DHLA PROMO

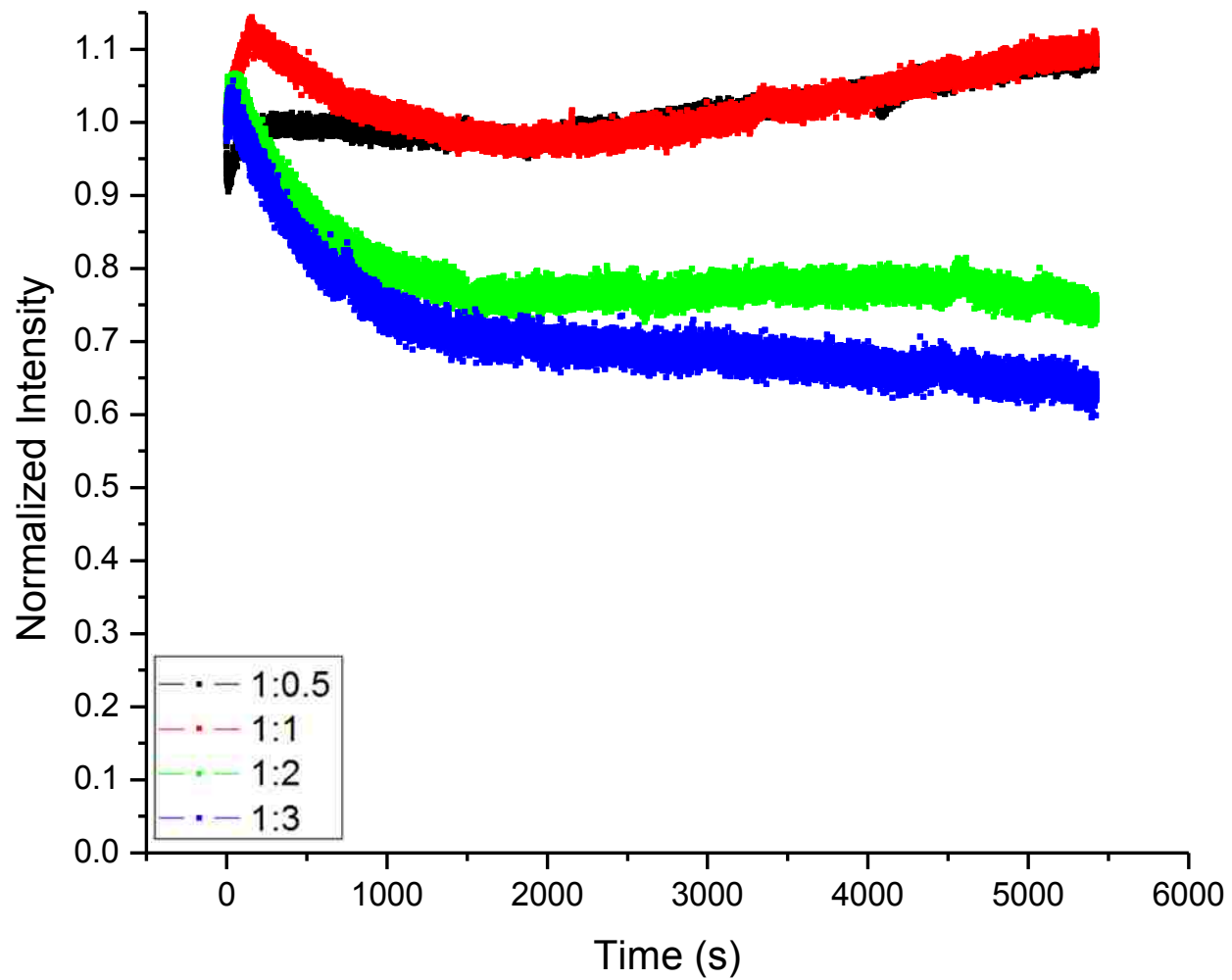
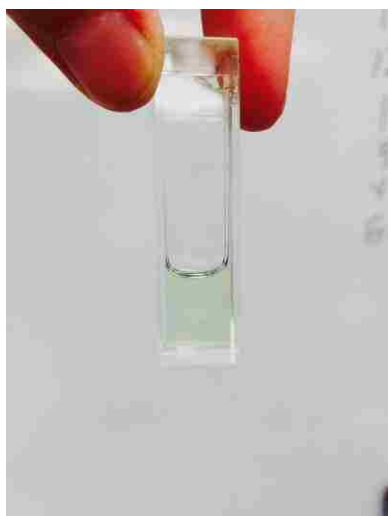


Figure 3.18: DHLA-PROMO normalized spectrofluorometer data.



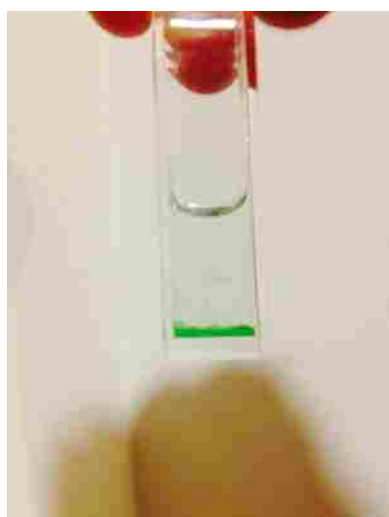
MPA-ATTO



DPA-ATTO



DHLA-ATTO



MPA-PROMO



DPA-PROMO



DHLA-PROMO

Figure 3.19: ATTO samples after measurement (top). PROMO samples showing aggregation after measurement (bottom).

3.4 Future Outlook

A better understanding of the mechanism of non-specific adsorption on QD surfaces can help expand their applications in other research. By understanding non-specific adsorption, there is a better chance of minimizing it and focusing on specific adsorption which can be used to functionalize QDs in a controlled way. The kinetic information about the exchange of surface ligand adds to our collective understanding of the non-specific adsorption. However, there are other ways to go about studying the exchange reaction of free thiolated dye reporters with the surface ligands and there are future projects to perform. For instance, what would be the effect of gradually increasing the concentration of the dye over an extended period of time? Perhaps a mixed ligand capping system could improve the overall resistance to non-specific adsorption. This project and others like it will continue to be important to further our understanding of these nanocrystals, because the future of QD research is very bright.

3.5 References

1. Drbohlavova, J., Quantum Dots - Characterization, Preparation and Usage in Biological Systems. *International Journal of Molecular Sciences*, 2009. 10: p. 656-673.
2. Efros, A.L. and M. Rosen, The Electronic Structure of Semiconductor Nanocrystals. *Annual Review of Materials Science*, 2000. 30(1): p. 475-521.
3. Masumoto, Y. and T. Takagahara, *Semiconductor quantum dots: physics, spectroscopy and applications*. 2002: Springer Science & Business Media.
4. Atkins, P. and J. de Paula, *Atkins' Physical Chemistry*: OUP Oxford.
5. Coffey, C.J.M.a.J.L., Quantum Dots: A Primer. *Applied Spectroscopy*, 2002. 56(1): p. 16A-27A.
6. C. B. Murray, D.J.N., and M. G. Bawendi, Synthesis and Characterization of Nearly Monodisperse CdE (E = S, Se, Te) Semiconductor Nanocrystallites. *The Journal of the American Chemical Society*, 1993. 115: p. 8706-8715.
7. Hines, M.A. and P. Guyot-Sionnest, Synthesis and Characterization of Strongly Luminescing ZnS-Capped CdSe Nanocrystals. *The Journal of Physical Chemistry*, 1996. 100(2): p. 468-471.
8. Smith, A.M., et al., A systematic examination of surface coatings on the optical and chemical properties of semiconductor quantum dots. *Physical Chemistry Chemical Physics*, 2006. 8(33): p. 3895-3903.
9. Deng, D., et al., Highly luminescent water-soluble quaternary Zn-Ag-In-S quantum dots for tumor cell-targeted imaging. *Physical Chemistry Chemical Physics*. 15(14): p. 5078-5083.
10. Bentzen, E.L., et al., Surface Modification To Reduce Nonspecific Binding of Quantum Dots in Live Cell Assays. *Bioconjugate Chemistry*, 2005. 16(6): p. 1488-1494.
11. Medintz, I.L. and H. Mattoussi, Quantum dot-based resonance energy transfer and its growing application in biology. *Physical Chemistry Chemical Physics*, 2009. 11(1): p. 17-45.

12. Selvin, P.R., T.M. Rana, and J.E. Hearst, Luminescence Resonance Energy Transfer. *Journal of the American Chemical Society*, 1994. 116(13): p. 6029-6030.
13. Clapp, A.R., et al., Fluorescence Resonance Energy Transfer Between Quantum Dot Donors and Dye-Labeled Protein Acceptors. *Journal of the American Chemical Society*, 2004. 126(1): p. 301-310.
14. Clegg, R.M., Fluorescence resonance energy transfer. *Current Opinion in Biotechnology*, 1995. 6(1): p. 103-110.
15. Willard, D.M., et al., CdSe/ZnS Quantum Dots as Resonance Energy Transfer Donors in a Model Protein-Protein Binding Assay. *Nano Letters*, 2001. 1(9): p. 469-474.
16. Yahia-Ammar, A., et al., Thin-coated water soluble CdTeS alloyed quantum dots as energy donors for highly efficient FRET. *Dalton Transactions*. 43(41): p. 15583-15592.
17. Ha, T., et al., Probing the interaction between two single molecules: fluorescence resonance energy transfer between a single donor and a single acceptor. *Proceedings of the National Academy of Sciences*, 1996. 93(13): p. 6264-6268.
18. Ha, T., Single-Molecule Fluorescence Resonance Energy Transfer. *Methods*, 2001. 25(1): p. 78-86.
19. Engel, T. and P. Reid, *Physical Chemistry*: Pearson Education.
20. Selvin, P.R., The renaissance of fluorescence resonance energy transfer. *Nat Struct Mol Biol*, 2000. 7(9): p. 730-734.
21. dos Remedios, C.G. and P.D.J. Moens, Fluorescence Resonance Energy Transfer Spectroscopy Is a Reliable "Ruler" for Measuring Structural Changes in Proteins: Dispelling the Problem of the Unknown Orientation Factor. *Journal of Structural Biology*, 1995. 115(2): p. 175-185.
22. Petryayeva, E., W.R. Algar, and I.L. Medintz, Quantum Dots in Bioanalysis: A Review of Applications Across Various Platforms for Fluorescence Spectroscopy and Imaging. *Applied Spectroscopy*. 67(3): p. 215-252.

23. R. Rossetti, S.N., L. E. Brus, Quantum Size Effects in the Redox Potentials, Resonance Raman Spectra, and Electronic Spectra of CdS Crystallites in Aqueous Solution. *The Journal of Physical Chemistry*, 1983. 79: p. 1086-1088.
24. Dabbousi, B.O., et al., (CdSe)ZnS Core/Shell Quantum Dots: Synthesis and Characterization of a Size Series of Highly Luminescent Nanocrystallites. *The Journal of Physical Chemistry B*, 1997. 101(46): p. 9463-9475.
25. Nie, W.C.W.C.a.S., Quantum Dot Bioconjugates for Ultrasensitive Nonisotopic Detection. *Science*, 1998. 281: p. 2016-2018.
26. Ute Resch-Genger, M.G., Sara Cavaliere-Jaricot, Roland Nitschke, and Thomas Nann, Quantum Dot Versus Organic Dyes as Fluorescent Labels. *Nature Methods*, 2008. 5(9): p. 763-775.
27. Gravel, E., Compact Tridentate Ligands for Enhanced Aqueous Stability of Quantum Dots and in vivo Imaging. *Chemical Science*, 2013. 4: p. 411-417.
28. Jaiswal, J.K. and S.M. Simon, Potentials and pitfalls of fluorescent quantum dots for biological imaging. *TRENDS in Cell Biology*, 2004. 14(9): p. 497-504.
29. Mandal, G., et al., Cadmium-free quantum dots as time-gated bioimaging probes in highly-autofluorescent human breast cancer cells. *Chemical Communications*. 49(6): p. 624-626.
30. Jose Aldana, Y.A.W., Xiaogana Peng, Photochemical Instability of CdSe Nanocrystals Coated by Hydrophilic Thiols. *The Journal of the American Chemical Society*, 2001. 123(36): p. 8844-8850.
31. Vladimir V. Breus, C.D.H., G. Ulrich Nienhaus Quenching of CdSe-ZnS Core-Shell Quantum Dot Luminescence by Water-Soluble Thiolated Ligands. *The Journal of the American Chemical Society*, 2007. 111: p. 18589-18594.
32. Susumu, K., et al., Enhancing the Stability and Biological Functionalities of Quantum Dots via Compact Multifunctional Ligands. *Journal of the American Chemical Society*, 2007. 129(45): p. 13987-13996.
33. Hiroko Takeuchi, B.O., Colin D. Heyes, Are Bidentate Ligands Really Better Than Monodentate Ligands for Nanoparticles? *Nano Letters*, 2013. 13: p. 4746-4752.

34. Algar, W.R., et al., The Controlled Display of Biomolecules on Nanoparticles: A Challenge Suited to Bioorthogonal Chemistry. *Bioconjugate Chemistry*. 22(5): p. 825-858.
35. Medintz, I.L., et al., Self-assembled nanoscale biosensors based on quantum dot FRET donors. *Nat Mater*, 2003. 2(9): p. 630-638.
36. Walling, M.A., J.A. Novak, and J.R.E. Shepard, Quantum Dots for Live Cell and In Vivo Imaging. *International Journal of Molecular Sciences*, 2009. 10(2): p. 441-491.
37. Liu, W., et al., Compact Biocompatible Quantum Dots Functionalized for Cellular Imaging. *Journal of the American Chemical Society*, 2008. 130(4): p. 1274-1284.
38. Dabbousi, B.O., et al., Langmuir-Blodgett Manipulation of Size-Selected CdSe Nanocrystallites. *Chemistry of Materials*, 1994. 6(2): p. 216-219.
39. Murphy, C.J., Peer Reviewed: Optical Sensing with Quantum Dots. *Analytical Chemistry*, 2002. 74(19): p. 520 A-526 A.
40. Jamieson, T., et al., Biological applications of quantum dots. *Biomaterials*, 2007. 28(31): p. 4717-4732.
41. Bera, D., et al., Quantum Dots and Their Multimodal Applications: A Review. *Materials*. 3(4): p. 2260-2345.
42. Alivisatos, A.P., Semiconductor Clusters, Nanocrystals, and Quantum Dots. *Science*, 1996. 271(5251): p. 933-937.
43. Lim, J., et al., Perspective on synthesis, device structures, and printing processes for quantum dot displays. *Optical Materials Express*. 2(5): p. 594-628.
44. Pong, B.-K., B.L. Trout, and J.-Y. Lee, Modified Ligand-Exchange for Efficient Solubilization of CdSe/ZnS Quantum Dots in Water: A Procedure Guided by Computational Studies. *Langmuir*, 2008. 24(10): p. 5270-5276.
45. Alivisatos, A.P., W. Gu, and C. Larabell, Quantum Dots as Cellular Probes. *Annual Review of Biomedical Engineering*, 2005. 7(1): p. 55-76.

46. Dyes, A.-T.F.L.a. ATTO 700. Product Data Sheet [cited 2015 6/23/2015]; Available from: https://www.attotec.com/attotecshop/product_info.php?language=en&info=p117_ATTO-700.html.
47. GmbH, P. PromoFluor 700P, Reactive Dyes. Instruction Manual 3/2014 [cited 2015 6/23/2015]; Available from: http://www.promokine.info/fileadmin/PDFs/All_PDFs/PK-PF700P-2-01.pdf.
48. Mattoussi, H., et al., Self-Assembly of CdSe/ZnS Quantum Dot Bioconjugates Using an Engineered Recombinant Protein. *Journal of the American Chemical Society*, 2000. 122(49): p. 12142-12150.
49. Li, Y., et al., White organic light-emitting devices with CdSe/ZnS quantum dots as a red emitter. *Journal of Applied Physics*, 2005. 97(11): p. 113501.
50. Yu, W.W., et al., Experimental Determination of the Extinction Coefficient of CdTe, CdSe, and CdS Nanocrystals. *Chemistry of Materials*, 2003. 15(14): p. 2854-2860.
51. Hiroko Takeuchi, B.O., Colin D. Heyes, Are Bidentate Ligands Really Better Than Monodentate Ligands for Nanoparticles? *Nano Letters*, 2013. 13: p. 4746-4752.
52. Hiroko Takeuchi, B.O., Colin D. Heyes, Are Bidentate Ligands Really Better Than Monodentate Ligands for Nanoparticles? *Nano Letters*, 2013. **13**: p. 4746-4752.